Physics – Uspekhi **61** (9) 846 – 870 (2018)

REVIEWS OF TOPICAL PROBLEMS PACS numbers: **42.50. – p**, 42.50.Nn, **42.55. – f**, 42.60.By

Plasmon nanolaser: current state and prospects

V I Balykin

DOI: https://doi.org/10.3367/UFNe.2017.09.038206

Contents

Abstract. In the last two decades, extensive research has been devoted to the development of new ultra-small lasers. The greatest progress has been made with semiconductor lasers. A fundamentally new approach to the miniaturization of lasers is based on using plasmon instead of photon fields. This review is devoted to an interesting and rapidly developing field, the physics of plasmon lasers. This area of research is the synthesis of plasmon and laser physics, which arose as a response to the need to reduce losses in plasmonic devices. Electrodynamics, materials science, laser physics, and other aspects of the subject under consideration are considered. A comparison of photon and plasmon nanolasers is given. The fundamental and technological problems of plasmon nanolasers are discussed. Their numerous applications are also considered.

Keywords: nanoplasmonics, surface plasmon, laser, nanolaser, spaser

V I Balykin Institute of Spectroscopy, Russian Academy of Sciences, ul. Fizicheskaya 5, 108840 Troitsk, Moscow, Russian Federation
Tel. +7 (495) 851 02 33. Fax +7 (495) 851 08 86
E-mail: balykin@isan.troitsk.ru

Received 12 June 2017, revised 1 September 2017
Uspekhi Fizicheskikh Nauk **188** (9) 935 – 963 (2018)
DOI: https://doi.org/10.3367/UFNr.2017.09.038206
Translated by M N Sapozhnikov; edited by A M Semikhatov

1. Introduction

Progress in modern technologies is to a great degree due to miniaturization, which has resulted in reducing the size of basic electronic devices to the level of a single-electron transistor [1]. Progress in the miniaturization of optical devices gave rise to the development of many research fields and practical applications [2]. These optical devices have been used in large-scale and high-speed communication networks since 1970 and became the basis for high-definition television and broadband Internet access. The next natural step in the development of photonics was the integration of optical devices. Two fundamental scientific problems in the integration of photonic devices are the localization of light and creation of nanolocalized laser sources.

In the last two decades, a wealth of research has been devoted to the development of new ultra-small lasers. The greatest progress has been achieved with semiconductor lasers [3–6]. A fundamentally new approach to miniaturization of lasers is based on the use of plasmon fields instead of photon fields. Plasmons appear due to the interaction of electron density oscillations with the electromagnetic fields exciting them. There are two types of plasmon oscillations and corresponding plasmon modes: (1) localized surface plasmons (on the surface of metal particles) and (2) surface plasmon polaritons (at the metal–dielectric interface). The fields produced by surface plasmons exponentially decrease away from the interface, which allows light to be concentrated at sub-diffraction limit scales. Correspondingly, electromag-

netic effects caused by these fields occur in the subwavelength region near surfaces on a nanometer scale. Therefore, the approach based on the use of plasmon fields instead of photon ones allows overcoming the diffraction limit on the laser size.

A plasmon nanolaser is a nanosize (in at least one dimension) quantum generator of nanolocalized coherent plasmon fields. A plasmon nanolaser that is nanoscopic in all three dimensions is called a spaser (Surface Plasmon Amplification by Stimulated Emission of Radiation) [7]. The idea of a plasmon nanolaser was first proposed by Sudarkin and Demkovich [8]. The possibility of creating a spaser was theoretically substantiated by Stockman and Bergman [7]. The concept of stimulated emission of plasmons was also discussed in [9] and reported in [10]. The idea of a plasmon nanolaser was further developed in theoretical papers [11–21]. The first experimental demonstration of a spaser was reported in [22]. By now, the operation of plasmon nanolasers has been demonstrated in numerous experimental studies [23–34]. Plasmon nanolasers have been described in a number of reviews [35–44].

The basic elements of a plasmon nanolaser, similarly to a photon laser, are the active medium, the active-medium pump source, and the resonator (Fig. 1). The active medium serves to excite plasmons in a resonator mode. An essential difference and advantage of a plasmon nanolaser compared to other existing sources of localized fields is that the plasmon nanolaser can operate in the regime of so-called 'dark' modes, which are weakly coupled to electromagnetic fields in the far zone. In other words, the plasmon nanolaser generates coherent, strongly localized fields. This is a considerable technological advantage because such a source of a nanolocalized electromagnetic field can affect quantum emitters (atoms, molecules, quantum dots) in the near field and efficiently excite them.

The use of plasmon nanolasers allows enhancing the synergy between electronics and photonics because a metal is the integral element of the plasmon nanolaser design and can also be used as electrodes as well as for efficient heat removal in integrated circuits.

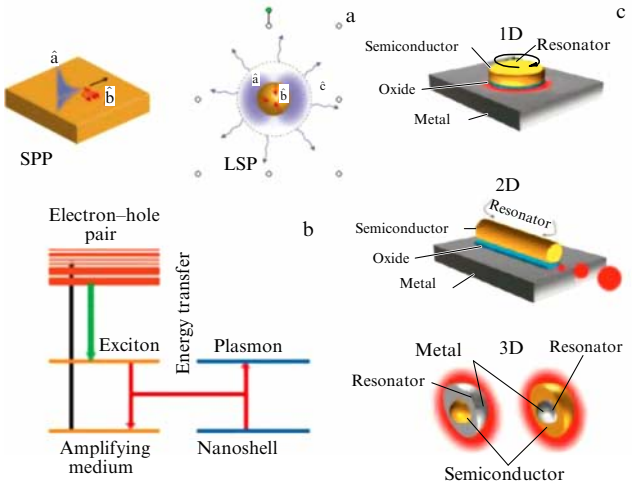

Figure 1. Illustration of a plasmon nanolaser. (a) Two types of plasmon excitations: propagating surface plasmons ($\hat{a}$) on a metal surface ($\hat{b}$) and localized surface plasmons ($\hat{a}$) near a nanoparticle ($\hat{b}$). (b) Illustration of the excitation energy transfer from the active medium to the plasmon mode of a spaser. (c) Three configurations of the plasmon nanolaser: one-dimensional (1D), two-dimensional (2D), and three-dimensional (3D) plasmon field localizations.

2. Resonator of a plasmon nanolaser

The *laser* resonator is a set of optical elements forming spatial and spectral modes for photons. Similarly, the resonator of a *plasmon nanolaser* is a set of metal/dielectric nanostructures forming spatial and spectral modes for plasmons. Two types of plasmons are distinguished (see Fig. 1): *localized* surface plasmons (LSPs) and surface plasmon polaritons (SPPs). These two types of plasmons are generated in a plasmon nanolaser using various types of resonators. There are three types of plasmon resonators: a 3D resonator for localized surface plasmons (three-dimensional field localization) and 2D and 1D resonators for surface plasmon polaritons (two-dimensional and one-dimensional localization of a plasmon wave).

2.1 Choice of the material for a plasmon nanolaser resonator

2.1.1 Metals. The choice of materials for plasmon resonators is a decisive factor for both ensuring plasmon nanolaser generation and achieving its optimal characteristics. Noble metals are currently the basic materials for experimental nanoplasmonics, because they have minimal losses among all the known natural materials. Losses are divided into two groups: (1) those caused by the presence of *free* conduction electrons and (2) those caused by *bound* electrons in a metal. Losses caused by conduction electrons appear due to electron–electron and electron–phonon interactions, as well as electron scattering by lattice defects and grain boundaries in polycrystalline metals. Losses caused by bound electrons appear when photons are absorbed upon an interband electronic transition to a highly excited state. Interband transitions cause considerable losses in metals in the optical wavelength range. Losses in metals significantly restrict progress in the development of a plasmon nanolaser.

Silver, as the main plasmon material, has minimal losses in the optical and near-IR spectral regions [45]. Losses can be considerably reduced by cooling a material to cryogenic temperatures [46]. For example, the mean free path of plasmon surface waves increases by 40–60% when decreasing the material temperature to cryogenic values [47].

Many resonators for plasmon nanolasers are based on thin metal films (silver, gold). As a rule, films less than 30 nm in thickness are no longer uniform, which results in additional resonator losses. In silver nanostructures, additional losses also appear due to the interaction of the metal surface with sulfur and chlorine inevitably present in the environment [48].

The next element after silver as regards minimizing the ohmic losses is gold. The technological advantage of gold over silver is its chemical inertia and the possibility of preparing uniform nanofilms 10 nm in thickness or less [49]. The presence of interband transition in gold introduces considerable losses at a wavelength of 470 nm. For this reason, gold is used in nanoplasmonics mainly in the near-IR region ($\lambda > 600$ nm) [50].

Other metals, for example, copper and aluminum, are also used in nanoplasmonics. Both these materials are less stable to the influence of the environment than noble metals are. The advantage of copper is that it is widely used in microelectronics. This allows considering copper as an alternative material in experimental nanoplasmonics from the standpoint of its possible practical applications. Among all the metals, copper has the second minimal electric conductivity, after gold. Its permittivity is similar to that of gold in the

spectral range above 600 nm [51]. A considerable disadvantage of copper is its rapid oxidation in air [52]. Copper oxides strongly impair the plasmon properties of nanostructures.

Aluminum as a plasmon material surpasses silver and gold in its optical properties in the blue and UV spectral regions [45]. Aluminum is the only material having a negative real part of the permittivity at wavelengths below 200 nm and therefore is a promising material for UV nanoplasmonics. Aluminum is not widely used in nanoplasmonics because of its oxidation in air (an Al_2O_3 layer ~ 3 nm thick is formed) and considerable interband transition losses at a wavelength of 800 nm [53].

We also note the fundamental potential of using alkali metals in nanoplasmonics. These materials surpass both silver and gold in their optical properties. However, their extremely high chemical activity significantly complicates their practical use [54].

Despite a huge number of studies with metals as plasmon materials, quite high losses in these materials in the optical range considerably restrict their applications [55, 56].

2.1.2 Other plasmon materials. Besides metals, there are many other materials that also have metallic properties and low losses, and can therefore be used in nanoplasmonics, in particular, for constructing a plasmon nanolaser resonator. Such materials include some semiconductors, transparent conducting oxides, transient metal nitrides, silicides, germanides, and 2D materials (such as graphene) [55, 56].

Among these materials, special attention is attracted to transparent oxides and transient metal nitrides as low-loss plasmon materials. Indium tin oxide and gallium-doped zinc oxide were shown to have metallic properties at wavelengths above 1.3 μm. Aluminum-doped zinc oxide was shown to have metallic properties at wavelengths above 1.8 μm. We note that losses in aluminum-doped zinc oxide at these wavelengths are a quarter of those for silver [57].

Titanium nitride (TiN) and zirconium nitride (ZrN) reveal metallic properties in the optical range above 500 nm. The plasmon properties of TiN are comparable to those of the best plasmon metals (Ag, Au) [58].

A promising approach in nanoplasmonics for searching for low-loss materials is based on *engineering* plasmon materials. A negative value of the imaginary part of the permittivity of a material is known to be responsible for losses in the material. It is also known that a small value of the imaginary part of the permittivity can be achieved either in the case of a small relaxation constant or at a low concentration of carriers. The decrease in the relaxation constant achieved by cooling materials to cryogenic temperatures considerably reduces losses; however, such devices are impractical for applications [46]. Therefore, an approach based on producing the required carrier concentration in the material seems more promising. Here, two possibilities exist: (1) the transformation of a semiconductor to a metal by doping and (2) the reduction in the carrier concentration in a metal by one method or another. Doping allows changing the carrier concentration in a semiconductor. A theoretical analysis in [54–56, 59] shows that to transform a semiconductor into a metal by doping, the carrier concentration must be no less than 10^{21} cm^{-3}. The doping method seems especially promising for obtaining silicon with metal properties [60, 61]. Heavily doped silicon is a material with strongly manifested plasmon properties [62]. However, obtaining plasmon properties in silicon at the telecommunication frequency remains a complicated and unsolved problem.

Apart from silicon, other materials have also been studied as regards obtaining plasmon properties in them: germanium, the III–V group materials, transparent conducting oxides, perovskite oxides, nonstoichiometric oxides, and sulfides [63].

Another approach to reducing optical losses in metals is based on decreasing the charge carrier concentration in a metal [64]. This is achieved by introducing nonmetal materials into a metal to reduce the total carrier concentration. However, such a process can change the initial electron band structure of the metal, resulting in the appearance of optical interband transitions, thereby increasing losses.

2.1.3 'Ideal' plasmon material. The reduction of losses in a metal by several orders of magnitude is a key problem whose solution will allow passing from academic studies in plasmonics to the development of devices for numerous practical applications [65]. A universal approach to the solution of such a problem is the synthesis of plasmonics materials. It is shown in [66] that losses in a metal can be reduced by several orders of magnitude by doubling the distance between neighboring atoms compared to that in natural metals. The approach proposed in [66] is based on the introduction of other atoms with closed electron shells between metal atoms for screening the electrostatic field. It is expected that losses will be reduced by several orders of magnitude in such artificial materials.

2.2 3D resonator for a plasmon nanolaser

A 3D plasmon nanolaser (spaser) is a nanoplasmonic device generating *localized* surface plasmons. Localized plasmons in a spaser play the role of photons in a laser, while a metal nanoparticle plays the role of the spaser resonator.

A 3D spaser can be constructed using a metal nanoparticle as a resonator with the replacement of its dielectric environment with an amplifying material. Plasmon generation is similar to lasing, the difference being that instead of photons in the laser mode, the spaser mode contains plasmons. Figure 2 illustrates the two simplest and most studied 3D spaser configurations: (a) with the amplifying medium at the center of a metal nanoparticle (*nanoshell configuration*) [67, 68] and (b) with the active medium in the form of the shell of a metal nanoparticle (*nanoparticle configuration*) [11, 69]. We note that other configurations of 3D spasers are also possible, for example, in the form of a split ring immersed in an amplifying medium (the split-ring

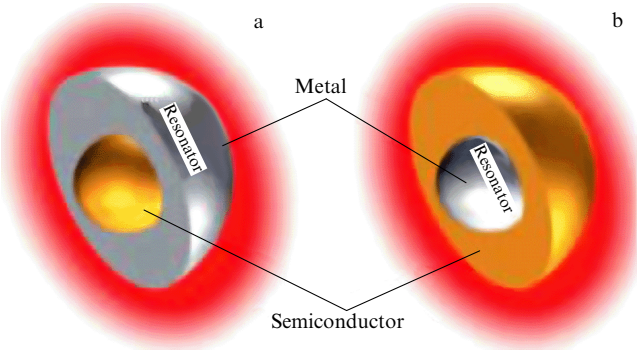

Figure 2. Two configurations of a 3D spaser: (a) with the amplifying medium at the center of a metal nanoparticle, (b) with the active medium outside a metal nanoparticle [22].

resonator), and also configurations based on dimers of short chains of metal nanoparticles.

The presence of a metal near the active medium makes the probability of transferring its excitation energy to the plasmon mode considerably higher than the probability of photon emission into free space: plasmon excitation in the mode occurs. If the next electron excitation in the active medium occurs for a time shorter than the plasmon lifetime in the mode, this plasmon stimulates the electron excitation transfer to the plasmon mode, and plasmons can accumulate in the given mode. The spaser operation depends both on the electromagnetic properties of the nanoparticle resonator (the nanoparticle size, the Q factor, and other parameters) and on the conditions of interaction of the nanoparticle plasmon mode with the amplifying medium. The spaser was first experimentally demonstrated in [22].

2.2.1 Eigenfrequencies of a spaser 3D resonator. The simplest 3D resonator for a spaser is a nanoparticle made of a noble or other metal. The size of this particle should be considerably smaller than the wavelength and lie in the range $l_{\rm nl} \ll R < l_{\rm s}$, where R is the nanoparticle radius, $l_{\rm nl}$ is the nonlocality radius, and $l_{\rm s}$ is the metal skin layer thickness. The nonlocality radius is determined by the distance covered by the electron moving with the Fermi velocity in the time equal to the light wave period $l_{\rm nl} \sim v_{\rm F}/\omega$. For most of the plasmonic metals, the skin layer has the thickness of the order of 25 nm. The nonlocality radius is $l_{\rm nl} \sim 1$ nm [70]. Thus, the size of the 3D plasmon resonator is from a few to a few dozen nanometers [11]. We also note that there is a technological restriction on the size of the 3D plasmon resonator imposed by the inhomogeneity of the nanoparticle material. In addition, the restriction on the minimal size also appears due to a drastic increase in losses during the scattering of electrons by the metal–dielectric interface with decreasing the nanoparticle size.

The eigenfrequencies of the 3D resonator of a spaser are determined by the resonances of localized plasmons in a nanoparticle, which are in turn determined by the size, shape, and material composition of the nanoparticle and its environment [71, 72]. The technology of producing nanoparticles with different shapes can be found in [73, 74].

The resonance collective oscillations of electrons in a metal nanoparticle are accompanied by high optical polarization with a strong absorption and scattering of radiation. The optical absorption and scattering for a homogeneous metal sphere in a homogeneous dielectric medium can be calculated by the Mie theory [75]. If the sphere diameter is considerably smaller than the wavelength, expressions for the absorption, $\sigma_{\rm a}$, and scattering, $\sigma_{\rm s}$, cross sections in the dipole approximation have the form [71]

$$\sigma_{\rm a} = \frac{18\pi V \varepsilon_{\rm m}^{3/2}}{\lambda} \frac{\varepsilon_2}{|\varepsilon + 2\varepsilon_{\rm m}|^2}\,, \qquad (1)$$

$$\sigma_{\rm a}(\omega) = 9\,\frac{\omega}{c}\,\varepsilon_{\rm m}^{3/2} V \frac{\varepsilon_2(\omega)}{\left[\varepsilon_1(\omega) + 2\varepsilon_{\rm m}\right]^2 + \varepsilon_2^2(\omega)}\,,$$

$$\sigma_{\rm s} = \frac{24\pi^3 V^2 \varepsilon_{\rm m}^2}{\lambda^4} \left| \frac{\varepsilon - \varepsilon_{\rm m}}{\varepsilon + 2\varepsilon_{\rm m}} \right|^2, \qquad (2)$$

where $\varepsilon = \varepsilon_1 + {\rm i}\varepsilon_2$ is the metal permittivity, $\varepsilon_{\rm m}$ is the permittivity of the medium surrounding the nanoparticle, and V is the nanoparticle volume. It follows from (1) and (2) that scattering is proportional to the particle radius to the sixth power, while losses are proportional to the radius to the third power. For small particles ($2a \ll \lambda$), the radiative decay of plasmon oscillations becomes insignificant, and the extinction cross section is completely determined by the dipole absorption. For example, for a gold particle 20 nm in size, the ratio of the absorption and scattering cross sections is $\sigma_{\rm a}/\sigma_{\rm s} \approx 100$.

It follows from expressions for the absorption and scattering cross sections that their maximum value is achieved for a nanosphere when the condition

$$\varepsilon_1(\omega) + 2\varepsilon_{\rm m} = 0 \qquad (3)$$

is satisfied. This condition determines the resonance frequency of a metal *nanosphere* with the permittivity ε_1 immersed in a medium with the permittivity $\varepsilon_{\rm m}$ [76]. The quasistatic approximation is valid only for small particles. For large particles, this approximation is invalid and the resonance frequency is no longer determined by the relation ${\rm Re}\,[\varepsilon] = -2\varepsilon_{\rm m}$ but also depends on the geometric characteristics of nanoparticles. This opens up additional possibilities for choosing the resonance frequency of a 3D resonator and hence the spaser generation frequency.

Modern nanotechnology methods can be used to produce nanoparticles with various shapes: spheres [77–79], hemispheres [80], spheroids [81], ellipsoids [82], nanoshells [83, 84], cubic nanoparticles [85, 86], triangular prisms [87], tetrahedrons [88], truncated tetrahedrons [89], nanorods [90, 91], three-dimensional pentamers [94], polyhedrons [95], nanostars [96], split-ring resonators (SRRs) [97, 98], and split-hole resonators (SHRs) [99]. All these nanoparticles can also be used as resonators for the spaser.

The best studied and frequently used nonspherical nanoparticles are nanorods. Nanorods provide a simple control of the central frequency of the plasmon resonance by changing the nanorod length, thereby tuning the plasmon resonance frequency of the nanoparticle to be in resonance with the emission frequency of quantum emitters of the active medium of the spaser.

2.2.2 Spectral width of a 3D spaser resonator. Another important characteristic of a nanoparticle as the spaser resonator is the width of the resonance determining the resonator Q factor. The spectral width of 3D resonator modes in the spaser is determined by the spectral width of plasmon resonances, which is in turn determined by the nanoparticle material and its shape. The permittivity of not too small metal particles is described quite well by the permittivity of a bulk material, which can be written as

$$\varepsilon(\omega) = \varepsilon_{\rm ib} - \frac{\omega_{\rm p}^2}{\omega(\omega + {\rm i}\gamma)}\,, \qquad (4)$$

where $\varepsilon_{\rm ib}$ is determined by interband transitions in the nanoparticle material, $\omega_{\rm p}$ is the plasmon frequency, and γ is the decay constant. Experimental data demonstrate a drastic increase in the width of the resonance and its shift with decreasing the particle size. The dimensional part is due to the behavior of quasi-free electrons in the nanoparticle interacting with the surface and to a break in the system periodicity because of the finite size of the nanoparticle. Two factors determine the dimensional dependence of the decay constant γ. The first is a geometric factor determined solely by the particle size. The second factor is determined by the nature of the nanoparticle–environment interface.

The geometric factor can be taken into account as a correction to the decay constant [100], and this part of the decay constant is inversely proportional to the nanoparticle diameter D:

$$\gamma_g = 2g_s \frac{v_F}{D}, \quad (5)$$

where v_F is the Fermi velocity and g_s is a constant of the order of unity. For nonspherical nanoparticles, a similar expression is valid in which the diameter D is replaced by the effective electron localization size. The widths of resonances in nanorods were successfully interpreted based on a classical ballistic model and quantum mechanical theory [101]. The predictions of the classical ballistic model and quantum mechanical considerations for nanoparticles with different shapes are inconsistent [102].

2.2.3 *Q* factor of the 3D resonator. An important parameter of both a photon and a plasmon resonator is its Q factor. The Q factor is determined by the number of coherent oscillations of the resonator mode field during which the resonator mode field preserves its phase and can accumulate energy from the external exciting field.

The resonator Q factor is defined as

$$Q = \frac{\omega}{2\gamma}. \quad (6)$$

For plasmon resonances, another definition

$$Q = \frac{-\mathrm{Re}\,\varepsilon_m(\omega)}{\mathrm{Im}\,\varepsilon_m(\omega)} \quad (7)$$

is also used.

It follows from quite general physical considerations that the Q factor of a spaser resonator based on a subwavelength nanoparticle is small. This follows from the relation between electric and magnetic field strengths [66] in a metal nanoparticle. The total energy of the system is a sum of the *potential* energy of electrons in the electric field and their mechanical *kinetic* energy. Half of the time, the energy is stored in the kinetic electron motion energy. The electromagnetic part of the field energy is stored mainly in its electric component, whereas the magnetic component is only an insignificant part of the total energy. The decay rate γ of electron oscillations in a metal is mainly determined by electron–phonon and electron–electron scattering and is of the order of 10^{14} s^{-1}. It follows from the conservation law for the total energy of the system that the field energy inevitably dissipates at the rate of 2γ.

The maximum Q factor for a silver particle is of the order of 100, while for a gold particle the Q factor does not exceed 20. Such low values of the Q factor for a 3D resonator impose stringent requirements on the parameters of the active medium of the spaser.

A specific feature of a nanoparticle as a spaser resonator is the appearance of amplification of the electromagnetic field near its surface with respect to the external electromagnetic field in which the nanoparticle is located. For nanoparticles smaller than the skin layer, the external electric field penetrates through the whole nanoparticle and produces in-phase oscillations of all the free electrons in the nanoparticle. Local fields excited near the nanoparticle exceed the external exciting field by Q times. The size of the amplified field region is determined by the nanoparticle size. The amplified field region can be changed by using a hybrid metal–dielectric nanostructure. The most thoroughly studied nanostructure of this type is the nanoshell, which seems to be one of the most promising geometric shapes of nanostructures for a spaser. The active medium in such a hybrid structure can be located in both the inner and outer regions of the nanoparticle. Nanoshells are widely used in nanooptics, in particular, as 3D resonators for spasers.

Silver surpasses all other materials as regards the electromagnetic field amplification in the blue spectral region. Other materials demonstrate comparable characteristics in different regions in the optical and IR spectral ranges [58].

2.3 2D resonator for a plasmon nanolaser

A 2D resonator for a plasmon nanolaser is a resonator for surface plasmon waves (SPWs) providing the required feedback for the operation of the 2D plasmon nanolaser. Surface plasmon waves propagate along the metal–dielectric interface or other metal structures, such as metal films or strips, metal particles of different sizes and shapes, holes in nanofilms, and surface slits or roughness. Surface plasmon waves are nonradiative waves localized along the interface of two media.

At present, SPW amplification and generation are demonstrated in different optical systems consisting of a metal–dielectric interface, nanofilms, nanostrips, and nanowaveguides integrated with amplifying media [23, 24, 26, 30, 39, 103–111]. Because the SPW properties greatly depend on the metal surface type and the surface nanostructuring extent, the properties of the 2D plasmon nanolaser are also determined to a considerable extent by the surface type.

2.3.1 Configuration of the 2D resonator for a plasmon nanolaser. Surface plasmon waves are restricted in the *transverse* direction at the subwavelength spatial scale, and therefore the construction of a 2D resonator for SPWs reduces to their spatial restriction *along* the surface. In this case, the resonator size in the propagation direction of plasmon waves cannot be smaller than the diffraction-limited value. In the most general case, the 2D resonator for a plasmon nanolaser is a certain type of metal waveguide nanostructured to produce feedback (similar to the laser resonator) for SPWs. As a 2D resonator, a metal waveguide is characterized by two main parameters: losses during the wave propagation and the degree of spatial localization of the waveguide mode [112, 113]. In general, when the mode is strongly localized, the wave losses during propagation are high. Losses are reduced by choosing the waveguide geometry for which a significant part of the mode energy is concentrated outside the waveguide metal [114, 115].

The construction of the resonator for a 2D plasmon nanolaser includes two stages: (1) the choice and preparation of a metal surface and (2) the nanostructuring of the metal surface to produce the feedback for plasmon waves.

(a) *Metal waveguide for a 2D resonator*. It follows from general physical considerations that the propagation length of plasmon waves increases as the fraction of the plasmon mode volume outside the metal increases. The development of the idea to decrease the fraction of the plasmon mode field outside the metal led to a structure in the form of a thin metal film in which two types of plasmon waves are possible: the long-range plasmon mode (long-range surface plasmon polariton, LRSPP) and the short-range plasmon

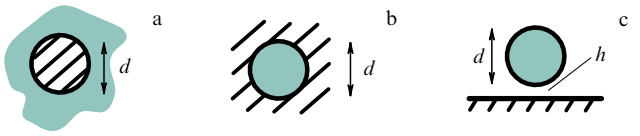

Figure 3. Three types of metal waveguides for the 2D resonator of a plasmon nanolaser: (a) metal nanocylinder, (b) nanochannel, and (c) hybrid waveguide.

mode (short-range surface plasmon polariton, SRSPP). The long-range plasmon mode in such a film is located mainly outside the metal, and its losses are hence considerably smaller than the plasmon wave losses on the metal–dielectric interface.

The further development of this idea leads to a structure representing a thin metal strip restricted in width or a metal nanowire forming a 2D nanowaveguide. The decrease in the film width (the reduction in the nanosystem symmetry) gives rise to a rich mode structure of the plasmon wave. In a width-restricted thin metal film, the fundamental mode and higher-order modes can be excited. Among them, there are modes with a small decay constant and a long propagation length. In particular, one of the modes does not have a cutoff frequency. A specific feature of this mode is that the spatial distribution of its electromagnetic field allows it to be excited by the simple focusing of laser radiation on the waveguide end [116]. As the waveguide thickness is decreased, this mode evolves into a transverse electromagnetic mode (TEM) of the dielectric surrounding the waveguide. Another interesting feature of this mode is its ability to sustain the leaky surface plasmon mode [117]. The leaky mode can be used to characterize both a passive metal waveguide and a plasmon nanolaser based on this waveguide.

(b) *Choice of a metal waveguide*. We consider the characteristics of plasmon waves in the waveguides of the three types most extensively studied in nanoplasmonics (Fig. 3): a waveguide in the form of a metal nanocylinder in a dielectric; a dielectric nanochannel in a metal; and a hybrid nanowaveguide in the form of a dielectric cylinder located along the metal surface at a certain distance from it [118–121].

A metal cylinder in a dielectric sustains a plasmon mode with subdiffraction spatial characteristics in a large range of its diameter values [118]. At the same time, the deep subdiffraction mode localization causes its strong decay. For example, for the mode area equal to 10% of the diffraction-limited area, the propagation length decreases by an order of magnitude compared to the propagation of the wave on a flat dielectric–metal surface. If a dielectric shell around the metal waveguide is added, the gain in the localization volume is insignificant, whereas the propagation length decreases by an order of magnitude. Such a waveguide sustains the plasmon mode only near the diffraction-limited mode area.

A dielectric nanochannel in a metal is a diffraction-limited waveguide having a cutoff frequency [118]. For a waveguide formed by a dielectric nanocylinder and a metal surface, the mode is formed due to hybridization of the photon mode of the nanocylinder and the plasmon wave of the flat metal surface. The wave propagation length in the hybrid mode can be large along with a considerable spatial localization of the field. Even in the case of the maximum mode localization (for small gaps), mode losses do not exceed plasmon wave losses on a flat metal–dielectric surface [118, 122, 123]. Moreover, in

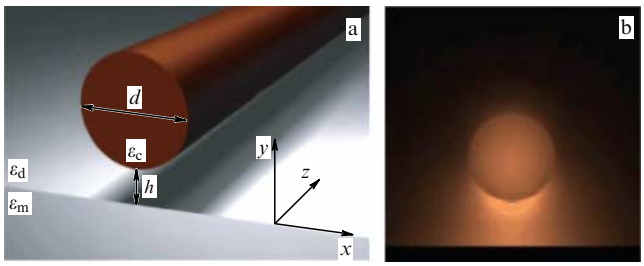

Figure 4. (a) Hybrid nanowaveguide consisting of a dielectric cylinder with diameter d located at a nanoscopic distance h from a metal surface. (b) The distribution of the hybrid mode field in the waveguide gap [124].

such a waveguide, additional field localization occurs due to the interaction of the surface metal charge with the surface polarization of the dielectric, resulting in a strong capacitive localization in the gap region.

The use of the hybrid mode in the semiconductor cylinder–metal surface configuration is extremely attractive for constructing the 2D plasmon laser, because the semiconductor cylinder can also be the active medium of the plasmon nanolaser (Fig. 4).

(c) *Chain of nanoparticles as a 2D resonator*. A chain of metal nanoparticles can be used as a waveguide for the electromagnetic field [125–131]. If a nanoparticle diameter is smaller than the wavelength of the external electromagnetic field, the response of each nanoparticle is described very well by the electric dipole model [71]. The resonance frequency of the dipole is determined by the nanoparticle material, its shape, and the permittivity of the particle environment. Due to the short-range interaction, the dipole field of one nanoparticle can excite plasmon oscillations in a neighboring nanoparticle [132]. If this is accompanied by efficient energy transfer between neighboring nanoparticles, this chain of nanoparticles represents a nanowaveguide.

Depending on the distance between nanoparticles, interactions of two types can appear in the chain. For a chain with the distance d between particles of the order of the excitation wavelength, the long-range interaction dominates, which depends on the distance as d^{-1} [71, 132]. For the interparticle distance considerably smaller than the excitation wavelength, the short-range interaction dominates, which depends on the distance as d^{-3}. The short-range interaction gives rise to eigenmodes of the chain of nanoparticles and the appearance of coherent modes with the wave vector along the chain. Energy transfer along the chain then occurs, which means that the chain is a nanowaveguide [133, 134].

Important parameters of a waveguide in the form of a chain of metal nanoparticles are the plasmon wave propagation lengths. Losses in a plasmon waveguide can be radiative and the ohmic losses in a metal. For particles significantly smaller than the wavelength, the radiative losses are negligible compared to ohmic losses. Experimental studies confirmed the possibility of channeling the electromagnetic energy via short-range interaction in the chain of metal nanoparticles over several hundred nanometers [135].

Waveguides based on nanoparticles allow creating complex plasmon elements with bent connections and beamsplitters without significant radiative losses. For example, during the propagation of a wave through bent (up to 90°) waveguide parts, the transmission of the waveguide part can be close to

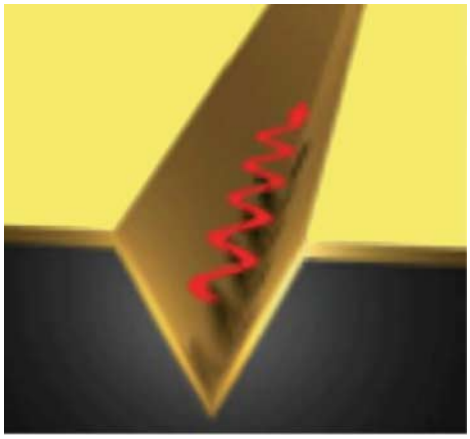

Figure 5. Groove in a metal for plasmon wave channeling.

100%. The development of nanotechnology methods has made it possible to create ordered chains of particles and to study their waveguide properties, including the possibility of their use for constructing a resonator for a plasmon nanolaser.

(d) *Slit and groove in a metal*. The possibility of plasmon wave channeling in a waveguide (Fig. 5) via a groove cut on the metal surface was first considered in [104, 136]. Plasmon waves along the groove channel were called *channel polaritons*. Channel polaritons have the properties of a spatially confined plasmon wave with subwavelength field channeling, relatively low losses in the single-mode regime, and the ability to propagate efficiently through the bent parts of the channel. Channel polaritons are also capable of the broadband transfer of signals [15, 137, 138]. As shown in [137], the propagation length of a plasmon wave along the channel can be large, albeit smaller than on the flat metal surface.

Channels of two types can be distinguished: in the form of a slit in a metal film and in the form of the letter V cut in a metal surface. The width of a V-groove cut in a metal monotonically decreases away from the metal surface. Because the field tends to localization in the region with the maximum effective refractive index, deep enough grooves can sustain plasmon modes near the groove bottom, where the effective refractive index is maximal [139]. The propagation length rapidly increases with decreasing the groove depth. In this case, the effective refractive index approaches its value in air, the spatial size of the mode increases, and it comes out from the groove. The propagation length also depends on the groove angle, increasing with this angle. In the limit case of a 180° angle, the plasmon wave becomes a wave on the metal surface [140].

For a channel in the form of a slit, channel polaritons originate from two plasmon waves in two half-planes, which become coupled waves at a sufficiently small distance between the half-planes [141–143].

2.3.2 Feedback in the 2D resonator. To build a 2D plasmon nanolaser based on a nanowaveguide, it is necessary to ensure feedback for plasmon waves along the waveguide. The field confinement along the waveguide is achieved by restricting the waveguide length in the nanolaser using a Fabry–Perot resonator [23, 144–147] or a coaxial resonator [4]. In the case of a metal rod waveguide [148, 149], the length of the nanolaser resonator is the length of the metal nanocylinder. When a semiconductor nanocylinder near a metal surface is used (a 2D hybrid-mode plasmon laser), the resonator length is the length of the semiconductor nanocylinder [124, 150, 151].

Nanocylinders in plasmonics have been studied in detail, both theoretically and experimentally [149, 152, 153]. The plasmon resonator in the form of a metal nanocylinder is characterized by the total length, the length of its cylindrical part, and the diameter and curvature radius of its ends. A nanorod in an external electromagnetic field has several resonances. The resonance at a small wavelength determines the dipole resonance, which is characterized by one node in the surface charge density [149]. The wavelength of the dipole resonance linearly depends on the total nanorod length down to small values, when the nanorod takes the shape of a sphere. In this case, the nanorod length is always considerably smaller than $\lambda/2$ [154]. Higher-order resonances correspond to shorter wavelengths.

Besides Fabry–Perot resonator schemes, some other schemes have been proposed and used to provide feedback in the 2D plasmon nanolaser. For example, a resonator can be constructed using distributed feedback [28]. Another approach uses the total internal reflection of plasmon waves [24, 25, 155].

An important parameter of a 2D plasmon nanolaser is the minimal size that can be achieved. The nanolaser size can be reduced by passing to the frequency range near the surface-plasmon resonance frequency. If the dipole mode of a nanocylinder away from the resonance frequency satisfies the half-wavelength condition, a dipole resonance in the short-wavelength part of the spectrum occurs for smaller nanorod lengths, thereby providing the smaller resonator size and the smaller volume of the plasmon mode [148, 156]. The resonance frequency is then independent of the nanorod length and its radius. The nanolaser size can be reduced to several dozen nanometers, as was demonstrated in [22].

2.4 1D resonator

The 1D resonator for a plasmon nanolaser is a nanostructured metal surface producing feedback for surface plasmon waves. The construction of the 1D resonator involves two stages: (1) the choice of a metal and creation of a metal surface and (2) the nanostructuring of the metal surface for providing the feedback.

2.4.1 Metal–dielectric interface. The simplest setup of the 1D resonator is based on using the metal–dielectric interface. A plasmon wave at the metal–dielectric interface is an evanescent wave exponentially decaying in both media with the distance from the interface [76]:

$$\begin{aligned} &E(z>0)\\ &\quad=(E_x^0,0,E_z^{\mathrm{d}})\exp\left[\mathrm{i}(k_{\mathrm{SPP}}x-\omega t)\right]\exp\left(-z\sqrt{k_{\mathrm{SPP}}^2-\varepsilon_{\mathrm{d}}k_0^2}\right),\\ &E(z<0)\\ &\quad=(E_x^0,0,E_z^{\mathrm{m}})\exp\left[\mathrm{i}(k_{\mathrm{SPP}}x-\omega t)\right]\exp\left(z\sqrt{k_{\mathrm{SPP}}^2-\varepsilon_{\mathrm{m}}k_0^2}\right), \end{aligned} \tag{8}$$

where E_x^0, E_z^{d}, and E_z^{m} are amplitudes of the corresponding components of electric fields in the dielectric and metal, ε_{d} and ε_{m} are permittivities of the dielectric and metal, and k_{SPP} is the

wave vector of the plasmon wave:

$$k_{\mathrm{SPP}}(\omega) = \frac{\omega}{c}\sqrt{\frac{\varepsilon_{\mathrm{m}}(\omega)\varepsilon_{\mathrm{d}}}{\varepsilon_{\mathrm{m}}(\omega)+\varepsilon_{\mathrm{d}}}}. \tag{9}$$

The normal components of the field are related to tangential components as

$$E_z^{\mathrm{d}} = \frac{\mathrm{i}k_{\mathrm{SPP}}}{\sqrt{k_{\mathrm{SPP}}^2 - \varepsilon_{\mathrm{d}}k_0^2}}\,E_x^0\,, \qquad E_z^{\mathrm{m}} = \frac{\mathrm{i}k_{\mathrm{SPP}}}{\sqrt{k_{\mathrm{SPP}}^2 - \varepsilon_{\mathrm{m}}k_0^2}}\,E_x^0\,, \tag{10}$$

$$E_z^{\mathrm{d}} = \mathrm{i}\sqrt{-\frac{\varepsilon_{\mathrm{m}}}{\varepsilon_{\mathrm{d}}}}\,E_z^0\,, \qquad E_z^{\mathrm{m}} = \mathrm{i}\sqrt{-\frac{\varepsilon_{\mathrm{d}}}{\varepsilon_{\mathrm{m}}}}\,E_z^0\,, \tag{11}$$

where E_z^0 is the amplitude of the field component at the metal–dielectric interface.

The real part of the wave vector determines the plasmon wavelength $\lambda_{\mathrm{SPP}} = 2\pi/\mathrm{Re}\,(k_{\mathrm{SPP}})$, which is always smaller than the wavelength in the dielectric, $\lambda_{\mathrm{SPP}} < \lambda = \lambda_0/\sqrt{\varepsilon_{\mathrm{d}}}$. The imaginary part of the wave vector determines the propagation length $L_{\mathrm{SPP}} = 1/\mathrm{Im}\,(2k_{\mathrm{SPP}})$. The typical propagation length is of the order of a few dozen micrometers. For example, the propagation length of a plasmon wave at the gold–air interface at the telecommunication wavelength of 1.55 μm is $L_{\mathrm{SPP}}/\lambda_{\mathrm{SPP}} \approx 220$. This value gives the upper bound for the Q factor $Q_{\mathrm{SPP}} = 2\pi L_{\mathrm{SPP}}/\lambda_{\mathrm{SPP}}$.

When the metal surface is not perfectly flat, a plasmon wave is scattered by surface irregularities, which reduces its propagation length. The total propagation length l_{tot} is determined as

$$\frac{1}{l_{\mathrm{tot}}} = \frac{1}{l_{\mathrm{ohm}}} + \frac{1}{l_{\mathrm{rad}}} + \frac{1}{l_{\mathrm{scat}}}\,, \tag{12}$$

where l_{ohm}, l_{rad}, and l_{scat} are contributions to the plasmon wave propagation length caused by ohmic, radiative, and scattering losses.

2.4.2 Dielectric–metal–dielectric film. The permittivity of metals is typically higher than that of dielectrics, $|\varepsilon_{\mathrm{m}}| \gg \varepsilon_{\mathrm{d}}$. As a result, the electromagnetic energy in a metal averaged over the period is always higher than the electromagnetic energy averaged over the period in a dielectric surrounding the metal [157]. This suggests that ohmic losses in thin metal films should be lower than at the metal–dielectric interface, and therefore thin metal films are preferable for building the resonator of a plasmon nanolaser.

Films can be prepared in two variants: (1) metal–dielectric–metal and (2) dielectric–metal–dielectric [158]. The dielectric–metal–dielectric structure is more practical for building the resonator of a plasmon nanolaser. On each surface of a metal film, its own plasmon mode can exist. As the film thickness is decreased, these modes can spatially overlap, resulting in the appearance of two new hybrid modes: symmetric and antisymmetric [159–161]. If the permittivity on both sides of the film is the same, the transverse component E_z (or H_y) in the guided symmetric mode is the symmetric component, whereas the longitudinal component E_x is antisymmetric. The opposite situation is observed for the antisymmetric mode. The longitudinal component of the electric field in the symmetric mode changes sign in the middle of the metal film (the field strength is zero). Because the decay is mainly determined by the longitudinal component of the electric field of the mode, the decay of the symmetric mode is weaker. Simultaneously with decreasing the mode decay, the mode localization degree decreases [158, 162]. The symmetric mode is called the long-range surface plasmon polariton (LRSPP), while the antisymmetric mode is called the short-range surface plasmon polariton (SRSPP).

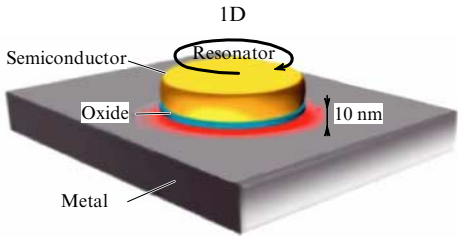

Figure 6. Configuration of the 1D resonator of a plasmon nanolaser with total internal reflection feedback. The nanolaser is formed by a semiconductor disc (active medium) located at a distance of 10 nm from a metal surface.

The field in a very thin film tends to escape from the metal, and its decay constant approaches its value in the dielectric: the decay constant tends to zero, while the propagation length tends to infinity, and hence the long-range plasmon mode evolves into a purely photon mode [163]. The weak decay of the long-range plasmon mode allows treating it as a mode of the resonator of a plasmon nanolaser. We note that losses of the long-range mode strongly increase in the absence of symmetry in the dielectric on both sides of the metal film. For example, for a 10 nm thick gold film immersed in benzocyclobutene, losses increase from 0.17 dB mm^{-1} in the symmetric situation to 0.4 dB mm^{-1} if the difference between refractive indices of the upper and lower dielectric media reaches 0.006 [164].

An example of a thin metal film with low losses is a silver film. For a 20 nm thick film immersed in an SiO_2 dielectric, the power decay constant at a wavelength of 1550 nm is $2\alpha = 0.0012$ dB μm^{-1} for the long-range plasmon mode and $2\alpha = 0.045$ dB μm^{-1} for the short-range mode. The decay constant sharply increases with decreasing the wavelength [162].

To date, a considerable number of theoretical and experimental studies have been performed on the amplification and generation of plasmon waves on thin metal films in the 1D resonator configuration [163–174]. The resonator of such a plasmon nanolaser consists of a size-restricted thin metal surface that is square or circular in shape [175, 176] (Fig. 6). Feedback in the resonator can be produced by the total internal reflection from the nanofilm boundaries (see Fig. 6). Feedback can also be obtained in the resonator configuration similar to a Fabry–Perot photon resonator [177].

3. Active medium of a plasmon nanolaser

As in a laser, the energy source of a plasmon nanolaser is the active medium. Compared to macroscopic lasers, small-size lasers (both photon and plasmon lasers) require amplifying media with a considerably higher gain. This is explained by the fact that mirror losses comparable to those in macro-

scopic lasers should be compensated in a much smaller volume, together with internal losses, which are often even higher than in macroscopic lasers. In addition, plasmon resonances providing a strong spatial localization of the electromagnetic field have a relatively low Q factor (no more than 100). These two circumstances impose strict requirements on the parameters of the amplifying medium.

The amplifying medium should compensate the attenuation of an electromagnetic wave during its propagation. An electromagnetic wave

$$E(x,t) = E_0 \exp\left[\mathrm{i}(k_x x - \omega t)\right] \tag{13}$$

propagating along the $+x$ axis is amplified when its wave vector k_x has a negative imaginary part. This condition is realized when the complex refractive index of the medium has a negative imaginary part, $\varepsilon = \varepsilon' + \mathrm{i}\varepsilon'' = n^2$. The optical amplification is expressed via the power gain γ relating the input I_{in} and output I_{out} powers as $I_{\text{out}} = I_{\text{in}} \exp(\gamma x)$. The power gain is defined in terms of the real and imaginary parts of the refractive index of the amplifying medium [178] as $\gamma = k_0 \varepsilon''/\varepsilon'$. In the case of a two-level amplifying medium with level populations N_1 and N_2, the gain dependence on the medium parameters is given by

$$\gamma(\omega) = A_{21} \frac{\lambda_0^2}{8\pi\varepsilon'} g(\omega) \left(N_2 - \frac{g_2}{g_1} N_1 \right), \tag{14}$$

where A_{21} is the Einstein coefficient, g_1 and g_2 are the degeneracies of the corresponding levels, and $g(\omega)$ is the frequency dependence of the spontaneous emission probability. If the condition $N_2 - (g_2/g_1)N_1 > 0$ is satisfied, the medium amplifies the wave in the spectral range determined by the function $g(\omega)$. It follows from (14) that to obtain a high gain, the concentration of emitters and the upper-level population should be high.

The gain required to reach the generation regime in a plasmon nanolaser depends on the type of plasmon waves and has the following values. For nondecaying *long-range surface plasmon waves* (LRSPWs) propagating along metal films 20 nm thick, the gain should lie between 1 and 200 cm^{-1}. For *short-range surface plasmon waves* (SRSRWs), the gain is already considerably higher and lies in the range from 1000 to 2000 cm^{-1}. For plasmon waves propagating along metal waveguides 50 nm thick, the gain should be between 2000 and 5000 cm^{-1}. For nanosize structures providing the subdiffraction *three-dimensional* localization of the field [the field mode volume $V_{\text{mod}} \ll (\lambda/2n)^3$], requirements for the medium gain are even stricter: the gain should lie in the range $10^3 - 10^5$ cm^{-1} [35, 38–44]. A comparison of plasmon resonator losses with the active medium gain allows estimating the fundamental possibility of achieving a lasing threshold in the system. The required high gain of the active medium and complications in the achievement of the high-Q mode in a plasmon nanolaser can lead to the appearance of parasitic *photon* lasing in the resonator.

Two types of excitation of the active medium of the plasmon nanolaser have been achieved to date: optical and electric.

3.1 Optical excitation

The choice of the active medium for optical pumping is rather limited. There are erbium-doped active glasses [180] and dye molecules [181–183].

Erbium-doped glasses are attractive for constructing a simple resonator + active medium scheme by doping a dielectric material with a low refractive index. However, the gain in such systems is low because of the low concentration of quantum emitters. For example, the gain at the telecommunication wavelength $\lambda = 1.535$ nm in heavily doped erbium glass is no more than a few cm^{-1} [180].

The use of dye molecules provides a considerable increase in the gain [169, 182, 184]. The amplification is possible in a broad spectral range (a few dozen nanometers) due to the complex vibrational–rotational energy level diagram of dye molecules. Dye molecules are pumped by lasers. The presence of double bonds in molecules provides the absorption of photons with wavelengths above 200 nm. Because of the Franck–Condon effect and fast intramolecular relaxation, the frequency of emitted photons is considerably shifted to the red (by a few dozen nanometers). Dye molecules can be readily dissolved in appropriate solvents, which become the environment of molecules. Dye molecules can also be placed into a solid dielectric medium (for example, polymers or glasses), which in turn can be integrated with metal nanostructures forming the resonator of a plasmon nanolaser.

There are a number of physical restrictions on the maximum gain of active media based on dye molecules [185]. These restrictions appear because of concentration-dependent effects such as the formation of dimers, concentration quenching restricting the maximum concentration of molecules in solution, and thus limiting the maximum density of molecules in the range from 10^{-4} to 10^{-7} mol l^{-1}. In addition, most of the dye molecules have long-lived triplet states into which excited molecules can transfer, resulting in a gain decrease. These factors set the maximum possible gain $\gamma \approx 10$–100 cm^{-1} [184].

The use of quantum dots (QDs) as the active medium allows increasing the gain considerably. Quantum dots are semiconductor nanocrystals larger in size than the lattice constant but comparable to the characteristic spatial size of the wave function of an exciton, an electron, or a hole. Although QDs contain thousands of atoms, their optical properties are similar to those of individual atoms because of the quantum spatial confinement of electrons at the nanometer scale.

Features of the optical absorption spectrum of QDs can be obtained from the expression for the probability of the dipole optical transition between the electron and hole states. The transition probability for the transition energy $\hbar\omega = E_{nl}^{\text{e}} + E_{nl}^{\text{h}}$ (above the band gap) is described by the expression

$$\alpha(\omega) \sim |p_{cv}|^2 \frac{1}{(4\pi/3)R^3} \sum_{n,l} (2l+1)\delta(\eta\omega - E_{nl}^{\text{e}} - E_{nl}^{\text{h}}), \tag{15}$$

where $E_{nl}^{\text{e,h}}$ are the final and initial state energies of the optical transition and $|p_{cv}|^2$ is the dipole transition matrix element squared. This expression gives the dependence of the optical characteristics of QDs on their size. As the size of nanocrystals is increased to ~ 40 nm, the spectrum transforms into the spectrum of a bulk material. The spectrum of a QD crystal is characterized by a sharp boundary of the energy band and a series of exciton states close to it.

The spectrum of a QD nanocrystal typically has considerable inhomogeneous broadening ($\sim 50-100$ nm) exceeding the homogeneous spectral broadening of an individual QD by more than an order of magnitude [186]. We also note that the

absorption spectrum of QDs at high excitation energies becomes a function without singularities and corresponds to the absorption spectrum of the bulk material.

There are two types of QDs: colloidal and epitaxial. They differ in the method of their preparation. Colloidal QDs are produced by the chemical synthesis of a nanometer structure from solution and consist of a core and a shell. Such QDs can be placed into a dielectric medium (for example, polymers), which in turn can be integrated with metal nanostructures forming the nanolaser resonator. In this case, the dielectric medium also affects the spectral characteristics of emitters and hence the parameters of the amplifying medium [187].

Epitaxial QDs (InAs) are prepared by the molecular beam epitaxy technique [188], their growth being based on the small difference between the lattice constants of InAs and GaAs crystals. When the InAs material is deposited on the GaAs surface during the growth process, a two-dimensional InAs layer is first formed. When the layer thickness reaches a certain value, the two-dimensional growth becomes the three-dimensional one because of the difference in lattice constants of InAs and GaAs crystals. As a result, the InAs nanocrystals (QDs) appear on the layer of a wetting InAs film. The InAs crystals are then covered by a GaAs layer. The surface density of QDs produced in this way is of the order of 10 μm^{-2} and higher. An individual QD has the shape of a lens about 3 nm in thickness with a diameter of 20 nm. The QD size and material determine the energy structure of the QD and its emission wavelength. The QD size can be varied in a broad range during its preparation.

The main advantages of using QDs as the active medium of the plasmon nanolaser are (1) the high radiative quantum efficiency of QDs, (2) the full compatibility of epitaxial QDs with the available semiconductor technology, (3) the possibility of placing QDs inside the resonator or near the nanostructure for controlling their optical characteristics, and (4) the stable optical properties of epitaxial QDs: the absence of bleaching effects and (or) blinking.

Active media based on QDs have a high gain. For example, $In_{0.53}Ga_{0.47}As$ QDs provide a gain of up to 2000 cm^{-1} at the telecommunication wavelength $\lambda = 1.5$ μm. Even higher gains can be achieved in epitaxial AlAs/GaAs QDs, where the extremely high gain of 68,000 cm^{-1} was obtained at 970 nm [189]. One of the important experimental advantages of QDs is that they are made of semiconductor materials for which numerous growth and processing methods and technologies have been developed in recent decades. Quantum dots can be excited both by optical radiation and by electric current.

3.2 Electric excitation

Plasmon nanolasers using inorganic semiconductors as amplifying media are pumped electrically and are compatible in design with modern semiconductor technology. This makes them the most technologically relevant sources of electromagnetic fields. In addition, semiconductor materials are robust, and therefore optical devices based on them have a long service lifetime. A semiconductor material can provide a compensation of losses exceeding 1000 cm^{-1}. Among the disadvantages of inorganic semiconductors used as active media is that in most cases they can operate only at cryogenic temperatures.

The best semiconductor materials for amplifying media are direct-gap semiconductors, such as the II–VI group semiconductor compounds. Among them, indium gallium nitride InGaN is the most promising amplifying medium with a broad amplification band. The bandgap of $In_xGa_{1-x}N$ $(0 \leqslant x \leqslant 1)$ can be varied from the IR to UV spectral range by changing the compound composition. The InN $(x = 1)$ semiconductor has the bandgap $\Delta E = 0.65$ eV, while the bandgap of GaN $(x = 0)$ is $\Delta E = 3.4$ eV. The InGaN semiconductor has a gain of about 10^4 cm^{-1} [190]. This makes it a promising material for building a plasmon nanolaser [39, 191].

The maximum gain of semiconductor materials at high pump powers is restricted by their thermal heating. High pump powers cause the heating of metal nanostructures forming the nanolaser resonator and can damage them [192]. Nanostructures are more readily subjected to thermal damage than the bulk metal, and microscopic thermally induced damage is observed in them at lower pump powers [193–195].

4. Characteristics of a plasmon nanolaser

Studies on the minimization of laser dimensions performed in recent decades revealed considerable physical differences between conventional macroscopic lasers and nanolasers [196–199]. In photon microscopic lasers, a significant role is played by amplified spontaneous emission, which changes the threshold behavior of the laser and increases the noise component of emission. In addition, the emission directivity of a microscopic laser considerably deteriorates when its size approaches the diffraction limit. Because of the small size, all these differences also exist for a *plasmon nanolaser*, and to a considerably greater degree. In addition, new features appear in the lasing regime inherent only in lasers of this type. These include: (a) a strong dispersion appearing due to the necessity of a high gain to achieve the lasing threshold and (b) a short optical response time of plasmon lasers due to a high gain and rapid spontaneous emission. Less manifested effects are also present, such as frequency pulling, gain guiding, and gain switching [36–44].

In photon lasers, lasing appears when the pump energy reaches a certain value (the lasing threshold) and its appearance is characterized by a number of physical effects such as (1) the spectral narrowing of output emission, (2) the appearance of directed emission, and (3) the appearance of spatial and temporal coherence. While these lasing features in macroscopic lasers are quite unambiguous, plasmon structures in nanolasers change the character of spontaneous emission of the active medium, and the passage to the lasing regime is not clearly manifested. The narrowing of the emission spectrum in plasmon nanolasers can occur even before the onset of lasing, which can lead to the incorrect interpretation of the operation regime of the device. When the amplifying medium maintains many modes in the nanolaser resonator, a change in the spontaneous emission rate can be more easily distinguished from real lasing, because the increase in the pump power then results in significant competition among the modes.

Because of the nanoscopic dimensions of a nanolaser and therefore its low emission power, the study of an individual nanolaser is an extremely complicated experimental problem. For this reason, studies are often performed with ensembles of nanolasers. However, nanolasers typically have different sizes, and therefore their lasing characteristics are different. For example, uncertainty appears in the value of the lasing threshold. In addition, effects occurring due to interaction

between individual spasers can also cause additional features in the behavior of spasers, which can be erroneously interpreted as the appearance of lasing.

The main characteristics of a nanolaser, such as the laser generation frequency, lasing threshold, pump power, and temporal response, are determined by the resonator geometry and material, the quantum mechanical characteristics of chromophores of the amplifying medium, and the method of energy coupling out of the resonator. The study of characteristics of individual nanolasers is complicated because of their nanoscopic size, whereas the study of ensembles of nanolasers (in which variations in geometric and other parameters lead to the spread of the lasing threshold and the broadening of the emission spectrum) complicates a comparison with theoretical models, which usually consider individual nanolasers.

4.1 Amplified spontaneous emission and lasing threshold

4.1.1 Field localization. Figure 7 schematically shows the three types of configuration of metal nanostructures used in plasmon nanolasers. Such metal nanostructures can support surface plasmon modes with different spatial localization degrees. A planar nanostructure (1D configuration) in the form of a metal–dielectric interface supports a surface plasmon mode restricted in one dimension. A structure in the form of a nanowire (2D configuration) supports a plasmon wave restricted in two dimensions. A structure in the form of a metal nanoparticle (3D configuration) restricts the field in all three dimensions.

A planar metal–dielectric structure and a thin metal nanowire are systems with one- and two-dimensional field localizations. Collective electron oscillations in such systems are related to a metal surface or a metal nanowire and are spatially localized in the direction perpendicular to the surface, while remaining waves freely propagating along surfaces. Therefore, such systems are nonresonance and support plasmon waves in the entire frequency range up to the plasmon frequency. Plasmon oscillations in metal nanoparticles are localized in all three directions. They have the resonance character and support plasmon oscillations at certain frequencies.

The localization degree of the electromagnetic energy depends on the configuration of metal nanostructures. For nanoparticles, the electromagnetic energy is confined to a volume considerably smaller than the diffraction limit $(\lambda/2n)^3$, where n is the refractive index of the nanoparticle environment. In the one-dimensional case (the metal–dielectric interface), the subdiffraction energy localization is possible in the direction perpendicular to the metal–dielectric interface. In this case, the localization degree depends on the optical characteristics of the metal and the dielectric and on the wavelength. Because of the spatially localized character of the plasmon surface wave, dispersion curves lie to the right of the corresponding light lines. At frequencies $\omega > \omega_p$, the propagation of radiation in the metal is possible. Between the regimes of coupled and radiative modes, there is a frequency range with purely imaginary values of the wave vector, where the propagation of waves is forbidden. For small wave vectors, the propagation constant of the plasmon wave is close to the value on the light line k_0, and the wave extends in the dielectric over many wavelengths.

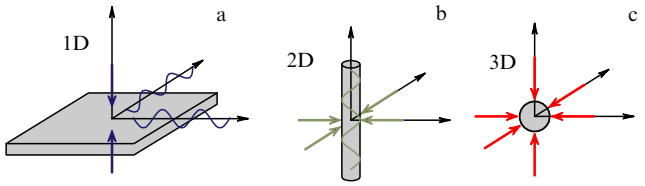

Figure 7. Metal nanostructures maintaining surface plasmon modes with different localization degrees. (a) one-dimensional configuration: metal–dielectric interface; (b) two-dimensional configuration: nanorod in a dielectric; (c) three-dimensional configuration: nanoparticle.

For large wave vectors, the wave frequency approaches the *plasmon boundary frequency* $\omega_{sp} = \omega_p/(1+\varepsilon_2)^{0.5}$. In the limit of the negligibly weak decay of the wave, the wave vector tends to infinity, the frequency approaches the *boundary frequency* ω_{sp}, the group velocity $v_g \to 0$, and the plasmon wave acquires an electrostatic character. In the 1D case, the maximum localization of the surface plasmon wave is reached near the surface plasmon frequency ω_{sp}. Surface plasmon waves in metal nanowires (the 2D case) are characterized by a considerably stronger field localization, with the localization degree depending on frequency as ω^{-2} [200].

4.1.2 Amplified spontaneous emission near nanostructures. When the nanostructure size is smaller than or comparable to the emission wavelength, the spontaneous emission rate of a quantum emitter located near the nanostructure can either increase or decrease compared to that in free space (the Purcell effect) [201]. This effect is quantitatively characterized by the Purcell factor $F = A/A_0$, where A is the spontaneous emission rate modified by the environment and A_0 is the spontaneous emission rate in free space. This effect affects a number of physical processes involved in nanolaser operation, because a strong spatial redistribution of spontaneous emission then occurs, with suppression of certain modes and amplification of other modes. This can in turn considerably change the lasing regime of the nanolaser. In the presence of feedback in the system (the nanolaser resonator), the spontaneous emission rate further increases proportionally to the resonator Q factor. In this case, the Purcell factor can reach significant values [200]. For 1D and 2D systems, assuming that the resonator Q factor is restricted only by internal losses in the metal, the Purcell factor reaches 10^2. The Purcell factor is large even at frequencies close to the surface plasmon frequency ω_{sp}, at which the maximum localization of the field is reached; however, losses also become maximal. For 3D systems (nanoparticle), the Purcell factor can be close to 10^6 and is limited by nonlocal effects [200, 202, 203].

4.1.3 Lasing threshold of a plasmon nanolaser. The strength of light interaction with a quantum emitter can be increased by decreasing the optical mode volume and increasing the resonator Q factor [201]. In photon lasers, this increase is achieved, as a rule, by using high-Q resonators [204–207]. In plasmon lasers, the increase can be achieved even at the low Q factor in a resonator with a sufficiently small mode volume.

Figure 8 shows the Purcell factor in a system consisting of a metal surface and a semiconductor nanorod as a function of the distance between the nanorod and the surface [146]. The left scale shows the Purcell factor and the right scale, the β factor. The β factor is defined as the fraction of spontaneous emission emitted in a certain resonator mode.

The maximum value of the Purcell factor in such a system is small, equal to 6. The maximum value of the β factor is 80%. For a gap smaller than 5 nm, the nonradiative

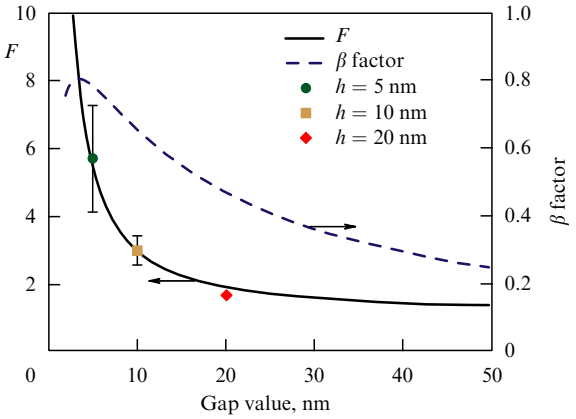

Figure 8. Purcell factor F in a hybrid mode formed by a metal surface and a semiconductor nanorod with a diameter of 120 nm as a function of the gap between them [146].

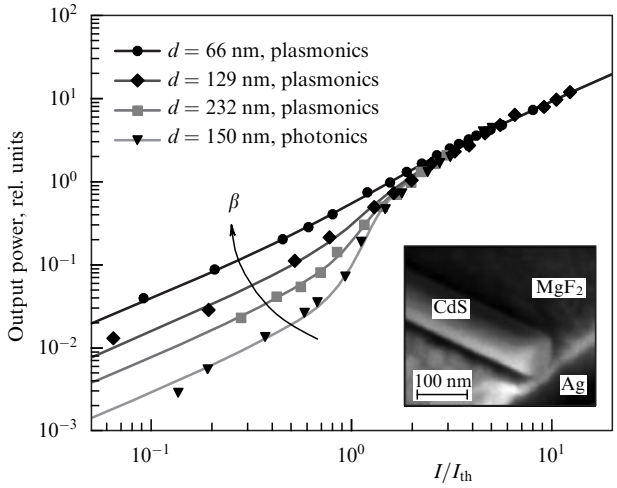

Figure 9. Illustration of a fundamental difference between the behaviors of photon and plasmon lasers: dependences of the output power on the pump intensity for photon and plasmon lasers. I is the pump intensity, I_{th} is the threshold intensity, and d is the nanorod diameter [146].

quenching on the metal surface leads to a drastic decrease in the β factor.

A high value of the Purcell factor ($F = 60$) was achieved for molecules inside the gap between a nanowire and a metal surface [147]. It was shown quite recently that the Purcell factor in plasmon structures can amount to 10–1000 [208–210].

The effect of increasing the emission rate in metal nanostructures is realized, as a rule, only for several modes, mainly for the most localized ones. For a plasmon nanolaser, this means that the strongest coupling of quantum emitters of the active medium is realized with the most localized modes of the nanolaser resonator. The coupling is quantitatively characterized by the β factor of spontaneous emission into a mode. The β factor plays an extremely important role in the threshold behavior of nanolaser lasing. Analysis of the lasing dynamics of the nanolaser shows that the lasing threshold is determined by the ratio of the total resonator losses to the β factor [200, 211]. While the β factor of the photon semiconductor laser is extremely small ($\beta < 10^{-3}$), it can be as high as $\beta \approx 0.8$ in a metal nanostructure [210, 212]. Therefore, lasing in a photon semiconductor laser is possible only in the case of low resonator losses, whereas lasing in a plasmon laser is also possible at high resonator losses [211, 213].

Figure 9 illustrates the difference between the behaviors of photon and plasmon lasers. The dependences of the output power on the pump power are shown for a photon laser formed by a CdS nanowire over a quartz surface and for a plasmon laser formed by a nanowire of the same material but over a metal surface [146]. We can see from Fig. 9 that the photon laser demonstrates a sharp transition between the regimes of spontaneous emission and lasing. In a plasmon laser, the transition to the lasing regime is manifested less clearly. At the same time, the output power of the plasmon laser strongly depends on the nanowire diameter. Such a difference in the behavior of these two types of lasers is explained by the large difference of β factor values for photon and plasmon lasers. This shows that the conventional definition of the lasing threshold is not valid for plasmon nanolasers.

Another specific feature of the plasmon laser is the strong dependence of its emission on lossy surface modes [214]. These modes dissipate energy in the metal, thereby greatly reducing the output power. Coupling with decaying surface modes considerably reduces the β factor, preventing the achievement of the lasing threshold of the spaser.

4.2 Emission linewidth of a plasmon nanolaser

The laser emission linewidth is one of the basic parameters of the laser and its change on passing from the spontaneous regime to stimulated emission clearly demonstrates the achievement of lasing: as the lasing threshold is achieved, the emission linewidth drastically decreases. In the case of a plasmon nanolaser for which the lasing threshold value is quite uncertain, the role of the lasing linewidth parameter is much more important than for a photon laser, because the evolution of the emission linewidth can indicate the onset of lasing [215].

The Townes–Schawlow theory predicts that the limit emission linewidth of the photon laser is proportional to the ratio of the resonator transmission bandwidth squared to the output power [216]. In most laser systems, this limit cannot be achieved for various reasons, and the emission linewidth greatly exceeds the theoretically predicted value. One of the reasons is fluctuations of the refractive index of the medium inside the laser resonator, which induce emission line broadening characterized by the linewidth enhancement factor [217].

A specific feature of the plasmon nanolaser compared to the photon laser is that the Q factor of its resonator (10–100) is extremely small. As a result, the emission spectrum of the nanolaser is determined not by the selective properties of its resonator but by the dispersion properties of the amplifying medium [203]. In [218], the spaser emission linewidth was studied by introducing the dispersion properties of the permittivity of the amplifying medium material. It was found that the emission linewidth of the plasmon nanolaser can be related to the linewidth $\Delta\omega_{TS}$ in the Townes–Schawlow theory as

$$\Delta\omega = (1 + \alpha^2)\Delta\omega_{TS}\,, \qquad (16)$$

where α is the linewidth enhancement factor in the plasmon laser resonator. Numerical simulation of the behavior of the

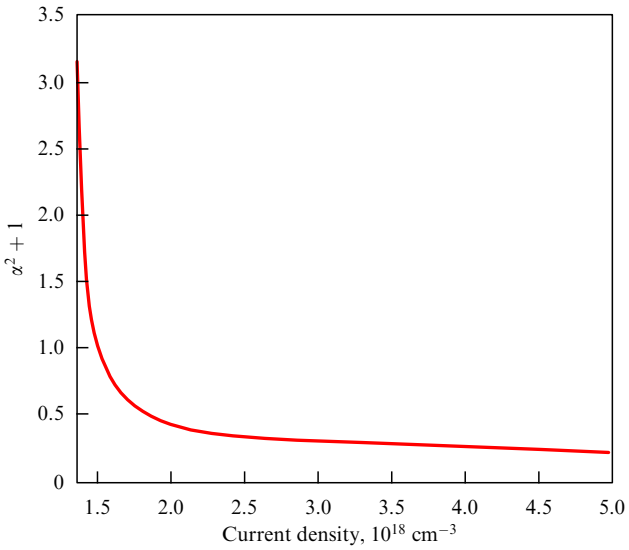

Figure 10. Dependence of the plasmon nanolaser linewidth on the pump current density [218].

emission linewidth of the plasmon nanolaser with the active medium representing an electrically pumped semiconductor showed that the linewidth in the lasing regime above the threshold monotonically narrows with increasing the pump power (Fig. 10), as predicted by the theory. This behavior of the spaser linewidth was confirmed experimentally [4, 219, 220].

4.3 Temporal characteristics of a plasmon nanolaser

Because of their small physical dimensions, plasmon nanolasers, like photon lasers, demonstrate dimensional changes of their characteristics, and to a considerably greater degree than photon lasers do. In addition, new features appear, such as strong dispersion due to the high gain required to obtain lasing and an ultrafast optical time response caused by the high gain and the increased spontaneous emission rate.

The physical reason of the ultrafast optical time response of the plasmon nanolaser is the short electron collision time in a metal, of the order of 100 fs. The ultrafast optical time response means the possibility of a large modulation frequency bandwidth of the plasmon laser. The amplification of the active medium can be switched at a time scale of the order of the plasmon lifetime, which is extremely short (about 10 fs). This means that emission of plasmon lasers can be modulated at the extremely high frequency of about 10 THz. The small spatial dimensions of plasmon resonators and the ultrafast temporal dynamics of the electromagnetic field of plasmon nanolasers allow their energy to be concentrated at the nanometer spatial scale and femtosecond temporal scale.

4.4 Radiative and nonradiative components of the electromagnetic field of plasmon nanolasers

Most of the energy of a 3D spaser is stored in the near field. The fraction of the electromagnetic energy inside a metal considerably exceeds its fraction in an adjacent semiconductor. The electromagnetic energy inside the metal rapidly dissipates into heat. Only a small part of the plasmon mode energy is released in the form of optical emission in the far zone. The characteristic energy dissipation time of a 3D spaser due to radiative losses is the Wheeler–Chu limit for a metal nanoparticle [221],

$$\tau_{\mathrm{rad}} = 3\left(\frac{\lambda}{2\pi a}\right)^3 \frac{\lambda}{c}\,, \tag{17}$$

where a is the nanoparticle radius. It follows from (17) that the radiative lifetime is $\tau_{\mathrm{rad}} = 8$ ps. On the other hand, for a subwavelength metal nanoparticle with a Q factor of about 15, the energy absorption time at a wavelength of 500 nm in a metal is $\tau_{\mathrm{abs}} = 25$ fs. Hence, only 0.003 of the total energy of generated surface plasmons is converted into optical radiation. Because radiation released in the form of the optical field constitutes a small fraction of the total energy, the near field can be of the greatest interest for practical applications of the spaser.

5. 3D plasmon nanolaser (spaser): experimental realization

A nanoparticle plasmon laser (spaser) can be built by replacing the dielectric medium surrounding a nanoparticle by an amplifying medium. Two schemes for realization a 3D spaser are possible: with the amplifying medium located outside and inside the nanoparticle (see Fig. 2). Theoretical estimates show that to obtain lasing under favorable physical conditions, a few hundred quantum emitters per nanoparticle are required [222].

The first experimental demonstration of a 3D spaser was performed with metal nanoparticles [22]. The metal nanoparticles were chemically synthesized gold nanospheres 14 nm in diameter covered with a dielectric silicon shell containing Oregon Green 488 dye molecules. The maximum of the emission spectrum of dye molecules was at 510 nm, coinciding with the wavelength of the plasmon resonance of nanoparticles. The total size of the 3D spaser was 44 nm. The resonator mode occupied a volume between the surface of a metal core (14 nm in diameter) and the external silicon shell (44 nm in diameter). The resonator Q factor was 14.8. The number of dye molecules per nanoparticle was 2.7×10^3. All the measurements were performed with an ensemble of spasers at a concentration of 3×10^{11} cm^{-3} in aqueous suspension.

The spaser consisted of a metal nanoparticle with a silicon dioxide shell containing dye molecules. This method involves a number of significant difficulties. First, dye molecules must be able to bind covalently with silicon dioxide via characteristic groups in the chemical structure of dye molecules [22]. Commercial dyes are not compatible with this method due to the absence of a functional group for covalent bonding [223]. Second, the method requires considerable technological experience in the preparation of a 'metal nanoparticle–dye-containing shell' with a concentration of dye molecules sufficient for compensating plasmon oscillation losses. Third, it is necessary to match the spectrum of the plasmon mode with the emission spectrum of dye molecules to provide the optimal transfer of the excitation energy of molecules to the plasmon mode of the nanoparticle. All these restrictions impede the experimental realization of a 3D spaser.

In [22], dye molecules were pumped by nanosecond laser pulses. Pulsed pumping facilitates the achievement of the lasing threshold. The spectral and threshold characteristics of the ensemble of spasers showed that emission was of the laser character: at low pump levels (Fig. 11), the measured spectrum was mainly determined by the spontaneous emis-

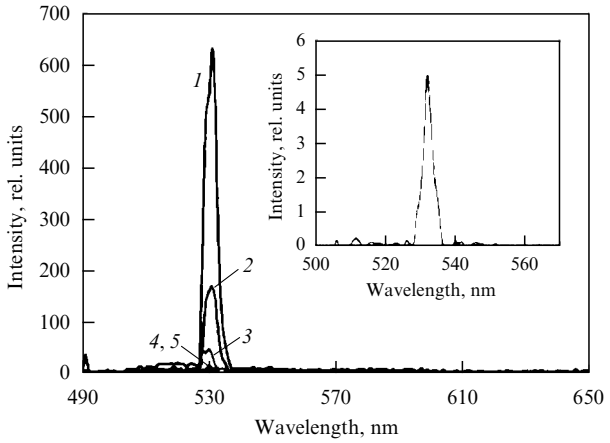

Figure 11. Spectra of a 3D spaser at different pump powers: 22.5 mJ (*1*), 9 mJ (*2*), 4.5 mJ (*3*), 2 mJ (*4*), and 1.25 mJ (*5*). Inset: emission spectrum of a 100-fold diluted solution containing spasers [22].

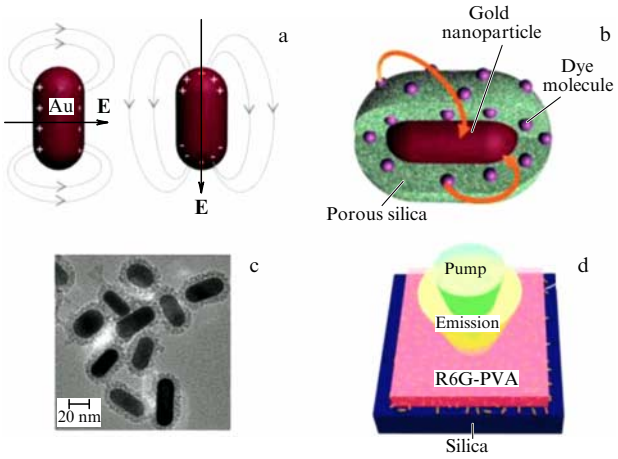

Figure 12. 3D spaser based on Au metal nanorods. Transverse and longitudinal nanorod modes. (b) Gold nanoparticle coated with a porous silica shell doped with dye molecules as the active medium. (c) Electron microscope photograph of a monolayer of gold nanoparticles with a porous silica shell. (d) Operation of an ensemble of spasers. (Rg6) Rhodamine 6G, (PVA) polymer.

sion of dye molecules. As the pump power was increased, a narrow peak appeared in the emission spectrum at a wavelength of 531 nm, which corresponds to the plasmon resonance of the nanoparticle. The dependence of the emission intensity on the pump power demonstrated the threshold type of lasing. The experimental lasing linewidth greatly exceeded the theoretical linewidth [224]. According to the experimental laser linewidth, the lifetime of the electromagnetic field in the resonator was about 200 fs, which is seven times greater than the estimated radiative lifetime of a plasmon resonator.

The operation of a 3D spaser with nanoparticles in the form of nanorods was demonstrated in [31] (Fig. 12). Nanorods maintain both transverse and longitudinal surface plasmon modes (see Fig. 12) and can therefore be used to control the spectral characteristics of the spaser resonator and to tune the spaser mode frequency to the maximum of the emission spectrum of the active medium. The wavelength of the longitudinal plasmon mode can be changed by changing the nanorod length. The longitudinal and transverse plasmon resonances were located at wavelengths of 520 and 610 nm. Calculations showed that the extremely small mode volume V of the nanorod resonator allowed achieving a high Purcell factor. The estimate of the longitudinal mode volume gives $V = 5.05 \times 10^{-24}$ m^3. Despite the low Q factor of the resonator, the ultrasmall mode volume provides the very high Purcell factor $F = 10^4$.

Creating a spaser based on nanorods involved several stages (see Fig. 12). Gold nanorods covered with a porous silica shell (Figs 12a, b) were deposited in the form of a monolayer on a glass surface (Fig. 12c). The monolayer of nanorods was then covered with a polyvinyl alcohol film containing Rhodamine 6G dye molecules, which were the active medium of the spaser. Dye molecules doped into a polymer have a higher photostability. In addition, the self-quenching of the dye fluorescence decreases and the fluorescence yield increases. The silica covering of gold nanoparticles prevents the formation of large molecular clusters [225]. Porous silica provides a more efficient interaction between the gold nanoparticles and surrounding dye molecules captured in silica pores. This in turn provides the efficient pump energy transfer from the active medium to the nanoparticle mode. The nanorods used in experiments had the following parameters: the nanorod diameter and length were 20 and 40 nm, respectively, and the shell thickness was 10 nm. The density of the nanoparticles was 1.6×10^7 mm^{-2}. Figure 12a shows an electron image of silica-covered gold nanorods.

The basic characteristics of the spaser were determined in experiments with spaser ensembles (Fig. 12d). Lasing was demonstrated in the wavelength range 562–627 nm with the emission linewidth 5–11 nm at room temperature.

Although these experiments were performed not with individual 3D spasers but with their ensemble, the authors of [22] believe that lasing observed in the experiments is the result of lasing of independent spasers. To date, the results in [22] have not been reproduced at other laboratories and have given rise to numerous critical comments. Various aspects of this work have been questioned by many researchers [31, 215, 226–229]. It was found in [229] that the pump rate required to obtain lasing is extremely high due to the very high dephasing rate of the plasmon laser, and it would be very difficult to achieve lasing under the experimental conditions in [22].

6. 2D plasmon nanolaser: experimental realization

A 2D plasmon nanolaser is a plasmon nanowaveguide with an active medium in the plasmon mode volume. To date, a great number of nanowaveguide structures have been investigated in nanoplasmonics, such as dielectric-loaded waveguides [105–107], nanorods [109], wedge nanowaveguides and nanochannels in a metal surface [103, 139], cylindrical metal–dielectric–metal waveguides [108, 230, 231], and hybrid plasmon metal–dielectric–semiconductor waveguides [124, 150, 151]. A 2D plasmon nanolaser can be built based on such waveguides by replacing a dielectric (on the metal surface) by active media (semiconductors, dye molecules, or quantum dots). The feedback along the wave propagation direction required for lasing can be obtained by using a Fabry–Perot resonator [23, 24, 26], distributed feedback [110, 111], or the total internal reflection effect [27, 175, 176]. Several 2D plasmon nanolasers setups have been developed.

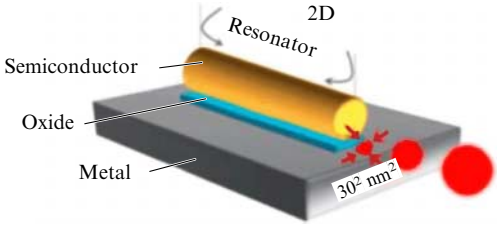

Figure 13. Illustration of a 2D plasmon nanolaser based on the dielectric-nanowaveguide–metal-surface structure. The nanowaveguide is a semiconductor nanorod located at a distance of several nanometers from a metal surface. Strong field localization appears in the gap between the nanorod and the metal surface. The nanorod is also the active medium of the nanolaser.

We consider a 2D hybrid dielectric–metal plasmon nanolaser. The main requirements for nanowaveguide structures used for constructing a 2D nanolaser is the 2D subdiffraction localization of plasmon waves and minimal plasmon wave losses. Among numerous 2D nanowaveguide structures, of considerable interest for building a 2D nanolaser is the hybrid dielectric–metal nanostructure [118] (Fig. 13). Such a nanostructure represents a semiconductor nanorod located at a distance of a few nanometers from a metal surface. The coupling between the photon mode of the dielectric waveguide and the surface plasmon wave on the metal surface produces a hybrid mode in the gap between the nanowaveguide and surface.

In the hybrid mode, most of the wave energy is concentrated in a nonmetal gap, providing strong field localization and simultaneously a large propagation length of the wave. If an amplifying semiconductor material is used as a dielectric nanowaveguide, such a system constitutes a 2D plasmon nanolaser [146].

Semiconductors used as amplifying media offer a number of advantages over other active media. First, semiconductors are electrochemically and photochemically stable; second, they have a high gain. Semiconductor materials serving as active media for nanolasers can be pumped both optically and electrically. In addition, semiconductor devices are reliable and durable and can be used for constructing various nanowaveguide structures.

The first successful demonstration of a 2D hybrid dielectric–metal plasmon nanolaser was reported in [146]. A dielectric nanorod was made of a CdS semiconductor [232], which was simultaneously the active medium and the resonator forming modes of the plasmon nanolaser in the longitudinal direction. The feedback in the resonator (along the nanorod) was provided by wave reflection from the nanorod ends due to the large difference between refractive indices of the semiconductor and air (Fabry–Perot resonator). The nanorod was located at a distance of several nanometers from the metal surface.

The active medium was optically pumped by a laser at a wavelength of 405 nm. Lasing was observed at a wavelength of 489 nm. The optical energy was localized in the metal–nanorod gap. The transverse size of mode localization was extremely small, about 10 nm. Lasing of the nanolaser was observed by wave scattering at the nanorod ends at a cryogenic temperature of the sample.

In the resonator configuration used, lasing can appear both in the photon and plasmon laser regimes. For the photon laser regime, a cutoff frequency exists, which appears for the nanorod diameter of 140 nm. The plasmon lasing regime can

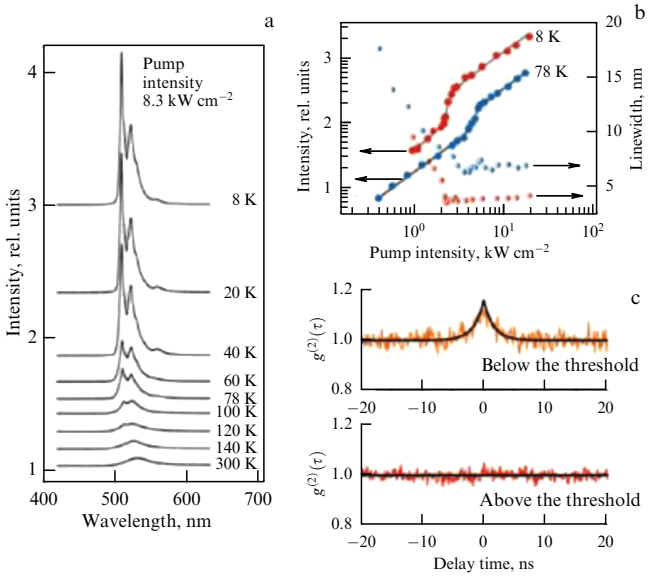

Figure 14. (Color online.) Emission characteristics of the 2D InGaN semiconductor plasmon laser. (a) Dependence of the nanolaser spectrum on temperature in the range 8–300 K. The lasing threshold is reached at 140 K. (b) Dependence of the nanolaser emission intensity on the pump power at 8 and 78 K. The curves demonstrate the lasing threshold. (c) Autocorrelation emission functions of the plasmon nanolaser [30].

also appear for a smaller diameter of the nanorod. Lasing was observed in experiments for the nanorod diameter equal to 52 nm. For such a nanorod diameter, only the plasmon lasing regime is possible.

In further experiments [25] with the hybrid structure based on CdS and Ag, lasing was already obtained in the optical spectral range at room temperature. The nanolaser field localization in the direction perpendicular to the surface was approximately 20 nm, while localization along the surface was of the order of 1 μm^2.

The same idea of constructing a nanolaser based on a hybrid mode but using a composite semiconductor material was realized in [27, 30]. A nanorod consisted of a core (an InGaN semiconductor) covered with a thin InN shell. The shell served as a gap between the nanorod and the metal surface.

To achieve continuous lasing in the plasmon laser, it is necessary to considerably reduce resonator losses. This was realized in [30] on a metal-surface–semiconductor-nanorod nanostructure in which the metal (Ag) surface was prepared with atomic precision, which considerably reduced losses in the plasmon resonator. The continuous lasing regime was achieved only at a low temperature. Figure 14 shows the temperature dependence of the nanolaser spectrum. At a temperature of 300 K, the spontaneous emission of an InGaN semiconductor is observed. Lasing appears at 120 K, when a small peak appears in the green region of the emission spectrum. At 8 K, a narrow spectral line appears at a wavelength of 500 nm. The experimental dependence of the output power on the pump power coinciding with theoretical calculations also confirms the achievement of lasing in the plasmon nanolaser. Measurements of the second-order correlation emission function before and after the onset of lasing also confirmed the appearance of lasing above the laser threshold.

Further development of this research resulted in the creation of an ensemble of single-mode nano-

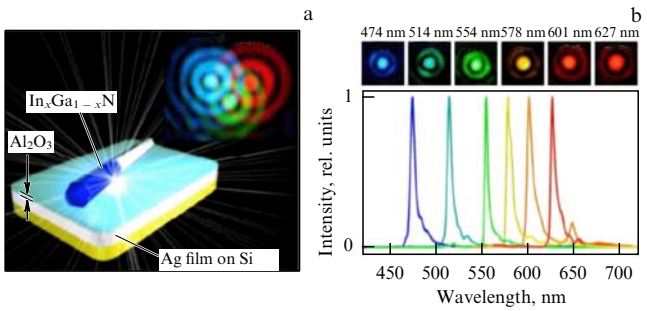

Figure 15. (Color online.) Simultaneous lasing of an ensemble of plasmon nanolasers at different wavelengths. (a) 2D nanolaser on a dielectric–metal hybrid nanostructure and the optical image of three nanolasers emitting at different wavelengths. (b) Emission spectra of nanolasers with different indium contents in nanoparticles: $In_xGa_{1-x}N$ $(0 \leqslant x \leqslant 1)$ [233].

lasers on a surface emitting simultaneously at different wavelengths [233]. The authors used semiconductor nanoparticles with different contents of indium in $In_xGa_{1-x}N$ $(0 \leqslant x \leqslant 1)$. It is known that the bandgap of a semiconductor can be varied from the near-IR to the UV region by changing its composition. For example, the bandgap of InN is $\Delta E = 0.65$ eV, while for GaN, $\Delta E = 3.4$ eV.

In experiments, several suspensions of nanoparticles with different contents of indium were deposited on a silver film. Nanoparticles of each type provided nanolasers emitting at specific wavelengths. Lasing at many wavelengths was achieved from an ensemble of nanolasers prepared by the successive deposition of nanoparticles with different contents of indium in InGaN on the silver surface. Figure 15a illustrates the setup of a hybrid dielectric–metal 2D nanolaser and the optical image of three nanolasers emitting at different wavelengths in the spectral range from the blue to the red. Because the physical dimensions of nanolasers are considerably smaller than the wavelength, their images in the figure are in fact diffraction pictures typical of point-like emission sources. Figure 15b shows the emission spectra of nanolasers between the blue and red spectral regions. The measured linewidth of nanolasers was considerably broader than that predicted by the Townes–Schawlow theory. The difference is explained by the ultrasmall size of the resonator and the additional broadening caused by the active medium noise.

7. 1D plasmon nanolaser: experimental realization

The 1D plasmon nanolaser is a 1D planar nanostructure consisting of a metal nanostructured surface with an adjacent dielectric used for amplification of a surface plasmon wave. As a 1D planar nanostructure, we can use the metal–dielectric interface, the dielectric–metal nanofilm–dielectric planar structure, or the metal–dielectric nanofilm–metal planar structure. The amplification and generation of surface plasmon waves have been demonstrated to date in all these planar nanostructures [26, 166, 175, 183].

7.1 1D plasmon nanolaser based on the metal–dielectric interface

Stimulated amplification of surface plasmon waves on a metal–dielectric interface was first observed in [169]. The metal was silver and the amplifying medium contained Rhodamine 101 and Cresyl Violet dye molecules. The amplification was obtained in the optical spectral range.

The 1D plasmon nanolaser was constructed on the metal–dielectric interface using whispering-gallery cavity modes to provide feedback for plasmon waves [176]. Such a nanolaser represents a 235 nm thick InP/InAsP/InP semiconductor disc prepared on a glass surface and covered with a silver layer. The semiconductor disc was made by electron beam lithography and dry etching. The disc was then covered by a silver layer. The nanolaser mode volume was $0.56(\lambda/2n)^3$. Lasing was obtained by optically pumping the active medium and was observed at temperatures between 8 and 80 K. Based on spectral measurements, the optical image of the mode, and its polarization properties, the generated mode was interpreted as the whispering-gallery plasmon mode on the bottom of the silver nanodisc.

7.2 1D plasmon nanolaser based on the dielectric–metal nanofilm–dielectric structure

A plasmon structure in the form of a symmetric metal nanofilm supports the two types of plasmon waves: a long-range surface plasmon wave and a short-range surface plasmon wave. The construction of a plasmon nanolaser with the use of a metal nanofilm and a long-range propagating surface plasmon wave is a simpler problem than the creation of a plasmon nanolaser on a metal surface, because the gain of the active medium required to overcome losses is lower in the former case [116, 160, 234, 235]. Such a configuration of the 1D nanolaser was demonstrated in [26]. The nanolaser comprised a metal (Au) waveguide nanofilm located inside the amplifying medium based on (InGaAs) quantum wells (Fig. 16). The waveguide length and width were 1 mm and 100 μm. A Fabry–Perot resonator was formed by the ends of the metal waveguide. The active medium was pumped by $\lambda = 1.06$ μm laser pulses. The narrowing of the emission line and the threshold behavior of the emission power confirm the appearance of lasing. Lasing was observed at room temperature at the telecommunication wavelength of 1.46 nm.

Continuous lasing in a nanolaser is prevented by heat release. This problem also exists for subwavelength photon lasers, where cw lasing is possible, as a rule, only at low

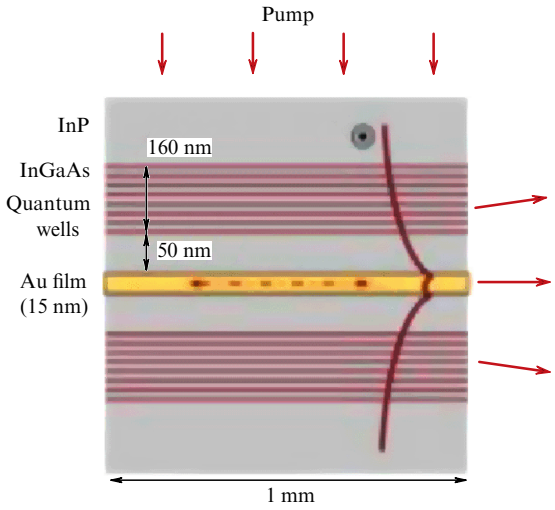

Figure 16. 1D plasmon nanolaser based on a planar metal waveguide and the active medium formed by InGaAs quantum wells [26].

temperatures. In [4, 110, 236], the continuous lasing of an electrically pumped 1D laser was demonstrated. However, the laser linewidth was rather large, being 3–4 nm [236]. This is quite a large value for most possible and expected applications of plasmon nanolasers, which require much narrower laser linewidths. Great efforts are being invested into the development of nanolasers operating simultaneously at (1) room temperature in (2) the cw regime with (3) the subwavelength mode size upon (4) electric pumping of the active medium. While all these goals have already been achieved separately, the simultaneous operation in all these regimes is still a difficult problem.

7.3 1D plasmon nanolaser based on the metal–dielectric nanofilm–metal structure

Of great interest in the development of the 1D nanolaser is a planar nanostructure in the form of a plane metal–dielectric–metal nanowaveguide in which the dielectric is replaced by the active medium. The metal–dielectric–metal waveguide provides subdiffraction localization of the mode in the transverse direction, and a major part of the mode volume can be filled by the active medium of the nanolaser. A nanowaveguide with a properly chosen width supports the propagating TM_{01} mode that spatially overlaps with the active medium of a spaser.

A metal–dielectric nanofilm–metal configuration can provide both photon and plasmon laser regimes, depending on the active medium thickness. As a plasmon laser, this configuration can operate only at a small thickness and cryogenic temperatures. At a greater thickness of the active medium, the photon lasing regime is possible. Because the photon mode losses are smaller, lasing can be obtained at room temperature.

The first planar nanolaser in the metal–dielectric nanofilm–metal configuration was demonstrated in [177]. The active medium was an InGaAs semiconductor, which was first covered with a 20 nm (SiN/InGaAs/SiN) silicon nitride layer and then with a silver layer. The silicon nitride played the role of an insulating layer, preventing the nonradiative deexcitation of the active medium by the metal. The ends of the nanolaser waveguide formed mirrors of a Fabry–Perot resonator. Due to the large length of the resonator (3–6 μm), its Q factor was rather high: $Q = 370$ at cryogenic temperature and $Q = 140$ at room temperature. The active medium of the nanolaser was pumped electrically.

The plasmon nature of lasing was confirmed by using a subwavelength thick active medium and observing the increase in the group refractive index of the laser mode upon decreasing the active medium width. The appearance of lasing was demonstrated by the narrowing of the laser emission spectrum with increasing pump power. Lasing with transverse field localization of about 50 nm was demonstrated.

Most 1D plasmon nanolasers operate at cryogenic temperatures. The necessity of using low temperatures is the main obstacle to their practical application. Considerable efforts are made to achieve the operation of plasmon nanolasers at room temperature. This requires ensuring low losses in the device, efficient feedback in the resonator, and high gain in the active medium. All these requirements must be satisfied in one device. The generation of plasmon waves in a planar structure at room temperature in the setup shown in Fig. 17 was demonstrated in [175]. The nanolaser resonator had the shape of a planar nanosquare with each side 1 μm in length and a thickness of 45 nm, made of the active medium (a CdS semiconductor) on a metal (Ag) surface. The active medium was separated from the metal by a thin (5 nm) insulator (MgF_2) layer. The so-called nanowaveguide metal–dielectric–semiconductor scheme was thus realized [175]. In this scheme, only plasmon modes are formed, because the total internal reflection regime for the chosen geometric parameters of the resonator is satisfied only for plasmon waves and not for photon waves. The total internal refection regime allows minimizing radiative losses in the resonator.

The construction provides a strong localization of the field with low ohmic losses in the metal, low radiative losses, and hence a high Q factor of the resonator. The strong field localization and the efficient feedback provided the high Purcell factor $F = 20$. A suitable choice of the resonator size also provided single-mode lasing with the nanolaser linewidth of 1.1 nm (Fig. 18).

Resonator mode losses in the planar metal–dielectric–metal configuration can be considerably reduced by using Bragg diffraction gratings as resonator mirrors. This allows lasing to be achieved at a lower pump level. In [110], lasing in a continuously electrically pumped nanolaser was observed at 80 K by using a Bragg diffraction grating. In [111], strong feedback was obtained by using a bandgap defect state inside a surface plasmon crystal. Lasing was observed under pulsed optical pumping at 77 K.

Lasing at room temperature, in the continuous regime and under electric excitation has been demonstrated in the metal–dielectric nanofilm–metal configuration in [237–239]. The best parameters of a nanolaser in the metal–dielectric–metal planar waveguide scheme were obtained in [237], where lasing was demonstrated at the telecommunication wavelength of

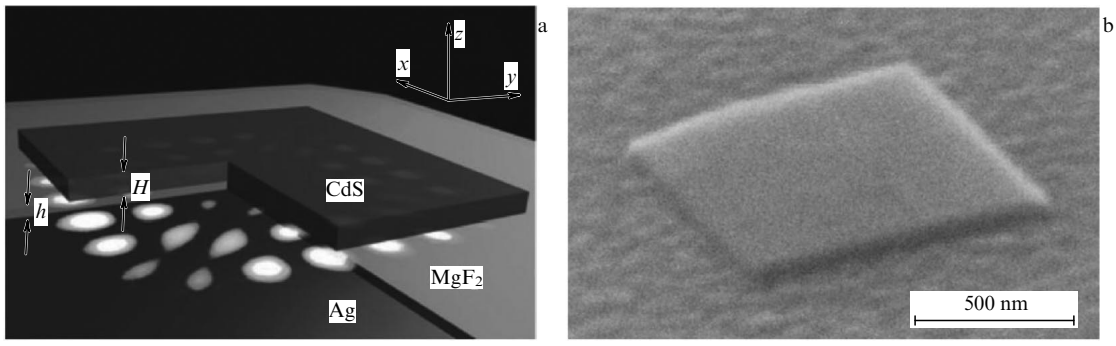

Figure 17. (a) 1D plasmon nanolaser based on a metal (Au) surface and a semiconductor active CdS medium operating at room temperature. The active medium is separated from the metal surface by an insulating material. (b) Electron microscope image of the nanolaser [175].

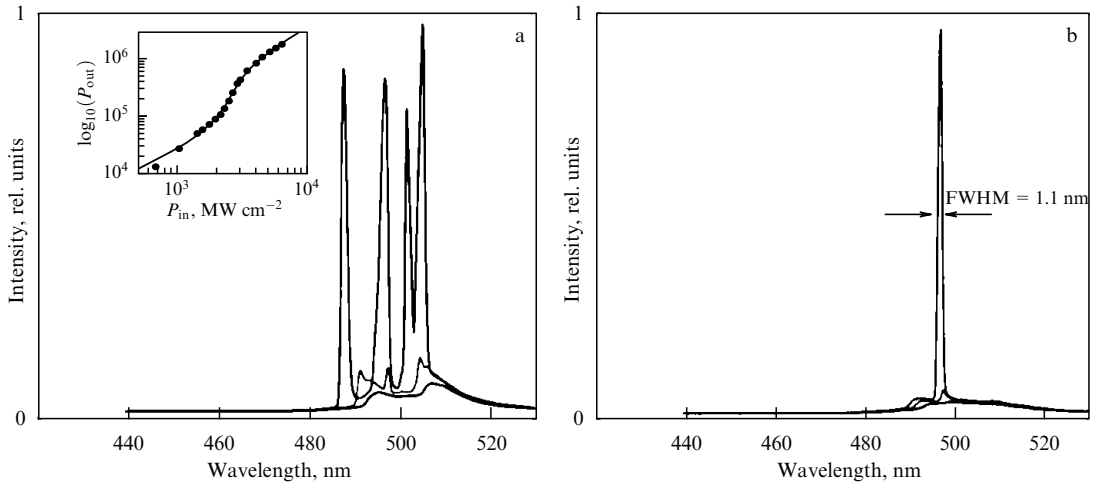

Figure 18. (a) Spectrum of the 1D plasmon nanolaser based on a silver surface and a semiconductor active medium. The evolution of the emission spectrum is shown from the broadband spontaneous emission to the narrowband lasing. Inset: dependence of the output lasing power on the pump power. (b) Single-mode lasing at room temperature.

1.6 μm at room temperature with a small mode volume $V_c \approx 0.67\lambda^3$. We note that this mode volume is still much greater than the mode volume for the 3D spaser.

7.4 1D plasmon nanolaser based on the plasmon crystal

A 3D nanolaser can be extremely small and can contain only several hundred atoms. However, the energy generated both in the near-field part and in the emission is extremely small. Presumably, the use of a regular structure containing separate nanoparticles (spasers) can allow increasing the generated power and simultaneously controlling the directivity of emission of an ensemble of spasers. The possibility of obtaining lasing from a periodic structure formed by metal nanoparticles was first discussed in [240]. Lasing was observed from an array of metal (Au) nanoparticles embedded into an organic film used as the amplifying medium. The narrowing of the emission spectrum was observed and the change in the emission power had a threshold, which confirmed the appearance of lasing.

Lasing was also observed in a complementary periodic structure consisting of a metal film with a periodic structure of nanoholes (plasmon crystal) [241] covered with the active medium (semiconductor quantum dots). The idea of using a plasmon crystal for generating plasmon waves was further developed in [242, 243], where more complex objects, optical nanoantennas, were used as nanostructures forming a plasmon crystal.

A regular structure of nanoparticles has resonances of two types: an individual particle and surface guided. Under certain conditions, the hybridization of these modes is possible [244]. For example, a chain of resonance nanoparticles [134, 245] allows the transport of plasmon excitations between nanoparticles. The guided propagation of excitation occurs with the transverse subdiffraction spatial field localization without radiative losses via the instantaneous 'quasi-electrostatic' dipole–dipole near-field interaction [135, 246]. The dispersion relation of such a guided mode can coincide at certain frequencies with the dispersion relation for free photons, which means that a chain of plasmon particles can be efficiently excited by an external light wave [247, 248].

The authors of [249] for the first time proposed to obtain directional lasing by using a 2D array of plasmon resonator particles. Directional lasing appears in such an array due to in-phase oscillations of nanoparticles. The amplification of the local field of an individual nanoparticle is manifested in the lasing of a plasmon crystal nanolaser via two effects. The first is spontaneous and stimulated amplification processes [242, 243]. The second is the band structure with a broad bandgap appearing in the plasmon crystal, which strongly modifies the distributed feedback in the plasmon crystal [250].

7.4.1 Plasmon crystal consisting of an array of nanoparticles. Figure 19 shows a plasmon crystal nanolaser [243]. The nanolaser consists of an array of Au nanoparticles on a glass surface covered by a polymer material layer that is used as the active medium. The polymer material consists of polyurethane and IK-140 dye molecules. Two physical effects are important in the behavior of this crystal: Wood's anomaly and the excitation of surface plasmon polaritons [251]. The crystal was pumped by 800 nm femtosecond laser pulses. The laser beam was directed at an angle of 45° to the plasmon crystal plane. The nanolaser operated at room temperature. The output emission was detected in the direction perpendicular to the plasmon crystal plane and demonstrated the threshold and narrowing of the spectrum. When the pump power exceeded the threshold, the directional emission at a wavelength of 913 nm with the spectral width $\delta\lambda = 1.3$ nm was observed. The beam divergence was 1.5°. The nanolaser emission was spatially coherent over a significant area of 50×50 μm^2, which confirmed the in-phase emission from individual nanoparticles.

To confirm the plasmon character of lasing, measurements were performed with a periodic structure of nanoparticles made of nonplasmon materials (titanium and titanium dioxide). No lasing was observed in that system.

Later, tunable and unidirectional lasing of a plasmon crystal nanolaser was observed in [252, 253]. The laser was tuned by changing the permittivity of the substrate on which the array of nanoholes was produced, and lasing was observed in the range from 862 to 891 nm with the emission linewidth of 1.5 nm.

7.4.2 Plasmon crystal consisting of an array of nanoholes. It was shown in [254] that the heating of a nanoparticle by laser radiation considerably depends on its shape and environ-

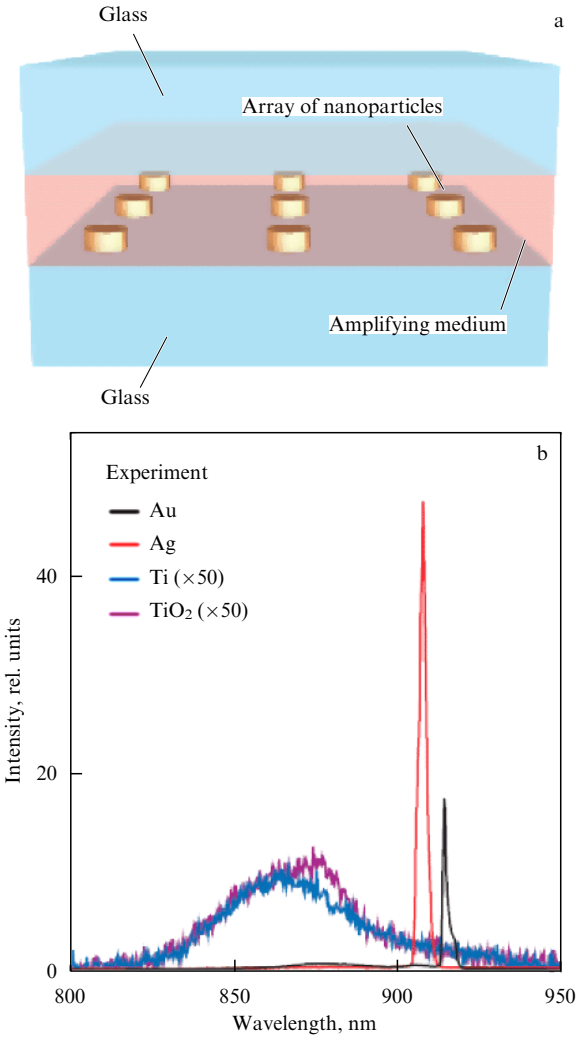

Figure 19. (Color online.) (a) Illustration of a plasmon nanolaser based on a plasmon crystal consisting of an array of nanoparticles embedded into the amplifying medium. (b) Emission spectrum of the plasmon nanolaser with plasmon crystals made of gold (black curve), silver (red curve), titanium (blue curve), and titanium dioxide (purple curve). Gold and silver plasmon crystals demonstrate lasing manifested in the increase in the emission intensity, the narrowing of the emission line, and the spectral shift of the laser line from the fluorescence line of the active medium [243].

ment. It was also found that the thermal damage of a metal nanostructure occurs at lower radiation intensities compared with the Babinet complementary structure produced in a metal film. Hence, under laser irradiation, a nanostructure in the form of a nanorod acquires the temperature a few orders of magnitude higher than the temperature of the complementary structure in the form of a nanoslit. Therefore, a plasmon crystal based on a structured nanofilm is preferable to an array of nanoparticles for the use in a nanolaser.

It was theoretically predicted in [225, 256] that directional coherent radiation can be obtained from a system consisting of a metal film perforated by a periodic array of nanoholes (plasmon crystal). The lasing of plasmon crystals with nanoholes was later experimentally demonstrated by using an array of metal holes [241, 257, 258]. A schematic of a plasmon nanolaser based on a plasmon crystal consisting of an array of nanoholes and the adjacent active medium is shown in Fig. 20 [241]. An indium phosphide (InP) plate was coated with a 105 nm thick indium–gallium arsenide

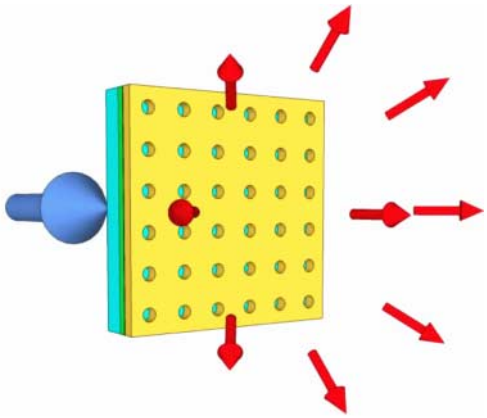

Figure 20. Schematic of a plasmon nanolaser based on a plasmon crystal consisting of an array of nanoholes [241].

(InGaAs) layer, which was then covered with a 15 nm thick InP layer. After that, a 5 nm thick silicon nitride (SiN) protective layer was applied. The protective layer was coated with a 100 nm thick gold film in which an array of nanoholes 160 nm in diameter was produced. The indium–gallium arsenide layer is the active medium of the nanospaser, which was pumped at a wavelength of 1.06 μm.

The achievement of lasing in the nanolaser was studied by the dependence of lasing power on the pump power. At low pump powers, emission at three frequencies determined by array resonances was observed. Above a certain pump power, the emission power in one of the three resonances (at 1480 nm) increased by more than three orders of magnitude, which was interpreted as lasing. Lasing was observed at cryogenic temperatures.

Lasing of a nanolaser based on a plasmon crystal with a periodic array of nanoholes in the optical range was observed in [258–260]. As the active medium, dye molecules in a polymer film [260] or solution [258] were used. Both emission spectrum narrowing and the lasing threshold were observed with increasing the pump power. Lasing was observed at room temperature.

8. Comparison of photon and plasmon nanolasers

8.1 Photon nanolasers

8.1.1 Minimal size of a nanolaser. The motivation for the miniaturization of lasers is the well-known incompatibility of the minimal achievable sizes of elements of silicon microelectronic devices (based on the use electrons) and optoelectronic devices (based on the use of photons). From the quantum mechanical standpoint, both electrons and photons are waves, and the fundamental restriction on the size of devices is determined by the corresponding wavelength. The electron wavelength is several orders of magnitude smaller than the photon wavelength (in the optical range), and therefore electron elements can be many orders of magnitude smaller than photon ones. This discrepancy of the dimensions is especially critical in integrated *electron–photon* devices, and because the laser is one of the main optoelectronic devices, the question about its minimal size is decisive in achieving integration of electronic and photonic devices.

In recent decades, studies on the miniaturization of photon lasers revealed significant differences in their char-

acteristics compared to macroscopic laser devices [198, 199, 261–263]. There are several fundamental restrictions on the minimal size of the laser that follow from the general physical principles of laser operation [264, 265]. For both photon and plasmon lasers, the field reproduction condition

$$r_1 r_2 \exp(2ikL) E_0 = E_0 \tag{18}$$

must be satisfied after the round-trip transit of a wave in the resonator, where r_1 and r_2 are the reflection coefficients of resonator mirrors, $k = k' + ik''$ is the complex wave vector, and E_0 is the amplitude of the wave field. Equation (18) gives two expressions for the minimal length of the laser resonator:

$$L_{\min}^{(1)} = \frac{\lambda}{2n_{\text{eff}}} m, \qquad m = 1, 2, \ldots, \tag{19}$$

$$L_{\min}^{(2)} = \frac{\ln(r_1 r_2)}{2k''} = \frac{-\ln(r_1 r_2)}{G_{\text{m}}}, \tag{20}$$

where λ is the wavelength in a vacuum, n_{eff} is the effective refractive index of the laser medium, and $G_{\text{m}} = \Gamma G_0$ is the modal gain equal to the active medium gain G_0 times the confinement factor Γ. The confinement factor is the ratio of the active medium volume to the resonator mode volume. Equation (19) determines the minimal size of a laser, which is equal to half the wavelength, taking the refractive index into account. The only possibility of further decreasing the longitudinal size of a laser is to increase the effective refractive index. For lasers made of semiconductors with high refractive indices (3.0–3.5), the first condition for the laser resonator length gives the minimal value 300 nm.

Further progress in laser miniaturization is possible only by passing to waves of a different type, namely, plasmon waves, for which the effective refractive index can be very high. The wavelength decreases especially strongly near the surface plasmon polarization resonance ω_{SR}, where the real part of the wave vector reaches its maximum [266].

The physical reason for the second restriction on the minimal length of the laser, Eqn (20), is the requirement of a finite size of the active medium to overcome resonator losses (mirror losses, diffraction losses, absorption and scattering of the wave). The minimal laser length $L_{\min}$ is achieved by using high-reflection mirrors and a high-gain active medium and choosing a resonator with the maximal confinement factor.

Conditions (19) and (20) determine the minimal length of a laser. Fundamental restrictions on the minimal transverse size of a laser also exist. Two laser configurations based on propagating waves are known. One of them is based on a Fabry–Perot resonator and the other is the waveguide version of the laser. In the first case, the 'transverse' size of the laser is determined by diffraction restrictions, and the minimal field size is of the order of the wavelength. In the waveguide type laser, the situation highly depends on the physical nature of the waveguide. In the case of a *dielectric* waveguide, the decrease in its diameter leads to an increase in the transverse size of the field outside the dielectric [267, 268], and the minimal size of the dielectric-waveguide–active-medium structure (and hence of the laser) is of the order of the wavelength. The use of a *metal photon* waveguide (a metal shell for a semiconductor photon laser) or a *plasmon* waveguide (for a plasmon laser) changes the situation quite significantly: the transverse size of the field mode can be much smaller than the wavelength. In this case, restrictions on the minimal transverse size appear due to two related factors: the field penetration into a metal through a finite depth (skin layer thickness) and the necessity of compensating high field losses in a metal due to the active medium occupying a finite volume.

8.1.2 Dielectric photonic nanolasers. An example of a photon nanolaser is the laser with a semiconductor nanorod as the active medium. The typical diameter of the nanorod lies in the range 10–100 nm and its length is 1–100 μm. The refractive index of semiconductor materials is in the range $\sim 2.5-3.5$. Therefore, a considerable difference between the refractive index of semiconductor materials and that of the air surrounding a nanorod provides a large confinement factor. In addition, a nanorod is also a nanowaveguide.

Another example of a photonic nanolaser is a photonic crystal laser. A photonic crystal can be both three-dimensional and two-dimensional. The characteristic size of a 3D photonic crystal laser is determined by the number of dielectric layers required to obtain a high reflection coefficient and is equal to a few micrometers. The size of 2D photonic crystal lasers in the crystal plane is also a few micrometers. The field restriction in the perpendicular direction is achieved due to total internal reflection, and the transverse size is several hundred nanometers.

8.1.3 Photon nanolasers with metal resonators. A considerable decrease in the mode volume in photon crystals is achieved by using metal coatings (mirrors) forming a resonator. The use of metal results in high resonator losses; nevertheless, the Q factor of resonators can reach large values up to several hundred [155], depending on the chosen resonator design. The optimization of the resonator parameters and the choice of the high-gain active medium simultaneously provides (1) continuous lasing at (2) room temperature (3) upon electric pumping [237].

Photon nanolasers with metal resonators use transverse electric (TE) or hybrid resonator modes. The miniaturization of such lasers leads to diffraction-limited dimensions in the range of a few hundred nanometers. A nanolaser consists of a metal capsule filled with a high-gain active medium [237]. There are also other configurations of photon nanolasers with metal resonators [269, 270].

A laser with an extremely small (picogram) mass was demonstrated in [271]. The volume of this laser was $V_{\text{eff}} = 0.019\lambda^3$, the laser diameter was 406 nm, and its thickness was 440 nm. The total mass of the laser was 0.6 pg. At 1420 nm, the laser emitted two fundamental modes of the resonator resembling the modes of oscillating electric and magnetic dipoles.

8.2 Plasmon nanolasers

Fundamental physical differences exist between photon and plasmon nanolasers: (1) the optical energy in plasmon nanolasers is amplified at spatial scales considerably smaller than the diffraction limit; (2) a strong coupling of radiation to matter in the nanometer resonator of a plasmon laser increases the rates of spontaneous and stimulated processes, making the plasmon laser a device with a fast response; and (3) the plasmon laser provides energy localization on the nanometer spatial scale and the femtosecond temporal scale simultaneously.

8.2.1 Plasmon nanolasers based on propagating plasmon waves. A photon nanolaser based on a dielectric rod as the active

medium has the minimal transverse size. A decrease in the nanorod diameter does not reduce the laser size because the mode field increases outside the nanorod [267, 272]. A further improvement in the transverse localization of a guided mode field is possible only by using a metal coating of a dielectric waveguide and propagating plasmon waves, i.e., by passing to the plasmon laser concept. In this case, a surface plasmon wave propagates along the waveguide and, as is well known, a strong localization of the electromagnetic field is possible near the resonance ω_{SPP} (the wavelength near the resonance decreases by more than an order of magnitude compared to the wavelength in a vacuum). As a result, the half-wavelength limit is reached along the wave propagation direction with no restriction on the transverse size (down to the skin layer thickness). However, in this case, maximum field losses appear near the resonance ω_{SPP}. This imposes stringent restrictions on the active medium gain and, as follows from (20), on the minimal nanolaser length. Both these factors require a compromise in choosing the parameters of the laser based on a dielectric with a metal coating [23].

8.2.2 Plasmon nanolasers based on localized plasmon waves. The only known configuration of a nanolaser in which all its dimensions can be significantly smaller than the wavelength is based on the use of a metal nanoparticle. In this case, the nanolaser size is determined only by the nanoparticle size (the resonator size) and the active medium gain capable of compensating losses in the nanoparticle. The nanoparticle laser is built using *localized* plasmon waves. The authors of [22] reported the generation of localized plasmon waves on a nanoparticle surrounded by an active medium with a total size of 44 nm. The active medium was optically pumped.

Implementing electric pumping (required for integrating nanolasers with other electronic circuits having nanosize components) is an even more complicated problem [215, 273]. The major fundamental difficulties appear due to the Purcell effect. It is known that the spontaneous emission rate increases with decreasing the resonator volume. To prevent the influence of the Purcell effect, the amplifying medium must supply enough energy to attain the stimulated emission of plasmons and hence lasing. The electric pump current for a metal nanoparticle nanolaser is so high that thermal damage of the laser material becomes possible. The electric pumping requires the development of new materials for active media and new resonator configurations capable of eliminating the parasitic influence of the Purcell effect.

Short relaxation times in a metal, a small resonator size, a short lifetime of surface waves, and a large Purcell factor in plasmon lasers lead to the attainment of very high modulation frequencies (in the terahertz range) of the plasmon nanolaser field [11, 200], which makes them attractive for many applications.

There is a fundamental difference between the polarization properties of emission from photon and plasmon nanolasers having the same nanoscopic dimensions. This difference is important and useful for identification of the physical nature of emission. As an example, we consider a nanorod resonator. In most cases, the polarization of a photon laser is perpendicular to the nanorod axis. The polarization of radiation for a plasmon laser is parallel to the nanorod axis. For example, for a nanorod diameter smaller than 150 nm, lasing appears mainly in the plasmon mode, while for a diameter exceeding 150 nm, the resonator can also maintain the photon mode, and photons are generated. Polarization differences in emissions allow the device type to be identified.

9. Applications

Studies in the field of nanolasers are motivated by the possibility of concentrating and manipulating the electromagnetic energy at the subwavelength spatial scale. In turn, the energy concentration on the nanometer scale allows amplifying both linear and nonlinear optical processes with the minimal energy down to the energy of single photons or plasmons. All this makes plasmon nanolasers promising sources of electromagnetic energy for numerous applications [76, 273, 274].

(1) *Photonic integrated circuits.* The most frequently mentioned possible application of nanolasers is photonic integrated circuits, which were first proposed by Miller in 1996 [275]. The most difficult problem in the development of photonic integration is the creation of efficient radiation sources on a chip. Plasmon nanolasers are potentially sources that not only can be integrated with other electronic and optical components but can also provide the operation of photonic circuits with an extremely broad modulation bandwidth. The temporal parameters of photonic systems based on nanolasers can significantly exceed the capabilities of modern electronic devices, because the capacitance load effect inherent in electric circuits is absent in optical systems.

The use of nanolasers as building blocks in digital photonic circuits has already been demonstrated in [276, 277]. Coherent subwavelength radiation sources are also of great interest for intercomponent connections [278, 279] and data storage [280].

We note that aside from radiation sources, the miniaturization of other passive plasmon elements required for photonic integrated circuits is also taking place. These include detectors, waveguides, and modulators with improved parameters and considerably reduced energy consumption [281].

(2) *Integrated electronic and photonic hybrid systems.* The incentive for laser miniaturization is the well-known incompatibility of the minimal dimensions of available silicon microelectronic and optoelectronic devices. This discrepancy of dimensions is especially critical in integrated electrooptic devices. Because the laser is a basic optoelectronic device, the question of its minimal size is decisive in the possibility of achieving integration of electron–photonic devices. A simple example of the possibility of miniaturization of photonic devices is the replacement of a standard optical fiber by a semiconductor nanowaveguide. In this case, the great contrast between refractive indices of the semiconductor nanowaveguide and air allows the size of a single-mode fiber to be reduced from a few micrometers (in the case of glass fibers) to a few hundred nanometers [267, 282].

(3) *Sensors.* Two parameters of plasmon lasers — their small size and strong field localization — make them attractive for the development of laser-based sensors. Nanolasers also provide the spatial diagnostics of objects on the nanometer scale. A strong localization of the electric field in a nanolaser allows amplifying weak, previously unmeasurable, optical effects and using them for diagnostics [283]. This improves the diagnostic sensitivity to the level of single molecules with nanometer spatial resolution [284–291].

Most of the plasmon detection schemes are based on *passive* plasmonics, with the sensitivity limited by large losses in a metal. It was shown theoretically that the use of *active* plasmonics (nanolasers) can significantly increase the detection sensitivity due to amplification of surface plasmon waves [9, 292].

Sensors based on active plasmonics measure the generated radiation intensity, which is sensitive to the presence of substances to be detected. It was shown in [293] that the use of a plasmon nanolaser as a sensor provides the detection of substances at the sub-part-per-billion level with subwavelength spatial resolution. A sensor of this type has been used for selective detection of various explosives, such as 2,4-dinitrotoluene, ammonium nitrate, and nitrobenzene [294].

An important advantage of plasmon nanolasers compared to traditional lasers in sensor diagnostics is their broadband emission, allowing diagnostics to be performed on the ultrashort time scale.

(4) *Biomedical applications*. High-sensitive sensors based on plasmon nanolasers are becoming an inherent part of biomedical applications. To date, the fluorescence of a molecular label remains the most powerful tool in biomedical studies for chemically and immunologically specific visualization of labeled molecules, viruses, cellular organelles, and living cells in complex biological systems [295]. A drawback of fluorescent labels for the visualization of biological objects is their insufficient brightness caused by the optical saturation and photobleaching [296]. Metal nanoparticles were proposed quite long ago as optical labels for biological studies. The advantage of metal particles as labels is the absence of photobleaching [297]. The disadvantage of metal particles is their broad absorption spectrum and the absence of fluorescence. This restricts the spectral selectivity of sensors based on metal nanoparticles both for visualization and for detection [298].

Results of recent studies [299] show that a plasmon nanolaser can be used as a universal tool in biomedical investigations. The use of plasmon lasers as labels eliminates the drawbacks of simple metal nanoparticles, because the lasing spectrum of a nanolaser is monochromatic and saturation is absent. In [300], a 3D spaser was used as a high-sensitive optical sensor. The spaser consisted of a gold nanoparticle 10 nm in diameter coated with a silica shell 12 nm thick, doped with uranine dye molecules as the amplifying medium. Uranine dye molecules are biocompatible with living cells. The laser linewidth was 0.8 nm. The spaser emission intensity exceeded the fluorescence intensity of a quantum dot label 380-fold. This spaser, biocompatible with living cells, is at present the brightest optical label.

Another biomedical application of nanolasers is based on the high energy density in the small optical mode volume of this laser. These properties allow using the nanolaser as an efficient manipulator and cutting tool for extremely precise surgery on biological tissues.

(5) *Optical communication and data storage*. Digital optical data processing is another field where nanolasers can find wide applications [301]. Because of the small size of nanolasers and the low Q factor of their resonators, the modulation frequencies of plasmon lasers lie in the terahertz range [19, 38, 302], which, with moderate power consumption, shows their potential advantages over high-frequency electronics methods. For the practical realization of such potential capabilities of plasmon lasers, it is necessary to solve numerous problems, such as directional data transfer and the separation of the input and output of optical elements [278, 303]. Experiments with nanolasers based on waveguides show that these problems can be successfully solved [182, 183, 304].

An important application of spasers is the field of informatics related to data storage: the sharply focused fields of plasmon lasers can be used for increasing the data storage density on carriers such as DVDs or hard discs [305, 306].

(6) *Super-resolution imaging, including biomedical imaging*. The high energy density and small size of the optical mode achieved in nanolasers can be used for nanoscopic imaging [307].

(7) *Ultrafast spectroscopy*. Plasmon lasers provide simultaneous energy localization on the nanometer spatial scale and the femtosecond time scale, which opens up possibilities for ultrafast spectroscopy.

(8) *Photolithography*. Strongly localized electric fields in plasmon lasers considerably increase the efficiency of the interaction of light with matter, which opens fundamentally new possibilities for photolithography. For example, the nanlocalized fields of plasmon lasers can be used for photolithography, eliminating restrictions encountered in experiments with conventional lasers [308–310].

10. Conclusions. Fundamental and technological problems of plasmon nanolasers

Numerous investigations of plasmon nanolasers have shown that their applications are promising. At the same time, many fundamental and technological problems concerning their commercial aspects remain unsolved. Some of them are listed below:

(i) An important characteristic for numerous applications of conventional lasers is the high directivity of their radiation. In plasmon lasers, the formation of radiation directivity is a problem due to diffraction

(ii) Many practical applications will require the stable operation of plasmon lasers, which assumes the availability of a simple and low-cost method for pumping the active medium of the laser. Electric pumping is preferable, which in turn requires solving the complicated problem of the construction of electric contacts for energy supply without deterioration of the optical parameters of the resonator mode.

(iii) To integrate plasmon nanolasers into photonic integrated circuits (large-scale integration), it is necessary to use technological methods for their construction based on the top-down principle, whereas most of the schemes for creating plasmon nanolasers are based on the bottom-up principle used in semiconductor microelectronics.

Acknowledgments

The author thanks A E Afanas'ev, A P Vinogradov, V N Zadkov, and P N Melent'ev for the useful discussions and O I Tat'yanchenko for her help in editing the manuscript. The study was supported by the Russian Science Foundation grant no. 14-12-00729.

References

1. Klein D L et al. *Nature* **389** 699 (1997)
2. Prasad P N *Nanophotonics* (New York: John Wiley and Sons, 2004)
3. Strauf S, Jahnke F *Laser Photon. Rev.* **5** 607 (2011)
4. Khajavikhan M et al. *Nature* **482** 204 (2012)
5. Schneider C et al. *Nature* **497** 348 (2013)
6. Dasgupta N P et al. *Adv. Mater.* **26** 2137 (2014)
7. Bergman D J, Stockman M I *Phys. Rev. Lett.* **90** 027402 (2003)

8. Sudarkin A N, Demkovich P A *Sov. Phys. Tech. Phys.* **34** 764 (1989); *Zh. Tekh. Fiz.* **59** 86 (1989)
9. Lawandy N M *Appl. Phys. Lett.* **85** 5040 (2004)
10. Protsenko I E et al. *Phys. Rev. A* **71** 063812 (2005)
11. Stockman M I *J. Opt.* **12** 024004 (2010)
12. Stockman M I *Phys. Rev. Lett.* **106** 156802 (2011)
13. Andrianov E S et al. *Opt. Lett.* **36** 4302 (2011)
14. Campbell S D, Ziolkowski R W *Opt. Commun.* **285** 3341 (2012)
15. Lisyansky A A et al. *Phys. Rev. B* **84** 153409 (2011)
16. Liu S-Y et al. *Opt. Lett.* **36** 1296 (2011)
17. Fedyanin D Yu *Opt. Lett.* **37** 404 (2012)
18. Andrianov E S et al. *Phys. Rev. B* **85** 165419 (2012)
19. Li D, Stockman M I *Phys. Rev. Lett.* **110** 106803 (2013)
20. Dorfman K E et al. *Phys. Rev.Lett.* **111** 043601 (2013)
21. Zhong X-L, Li Z-Y *Phys. Rev. B* **88** 085101 (2013)
22. Noginov M A et al. *Nature* **460** 1110 (2009)
23. Hill M T et al. *Opt. Express* **17** 11107 (2009)
24. Oulton R F et al. *Nature* **461** 629 (2009)
25. Ma R-M et al. *Nature Mater.* **10** 110 (2010)
26. Flynn R A et al. *Opt. Express* **19** 8954 (2011)
27. Wu C-Y et al. *Nano Lett.* **11** 4256 (2011)
28. Marell M J H et al. *Opt. Express* **19** 15109 (2011)
29. Sorger V J, Zhang X *Science* **333** 709 (2011)
30. Lu Y-J et al. *Science* **337** 450 (2012)
31. Meng X et al. *Nano Lett.* **13** 4106 (2013)
32. Yang A et al. *Nature Commun.* **6** 6939 (2015)
33. Hayenga W E et al. *Optica* **3** 1187 (2016)
34. Chou Y-H et al. *Nano Lett.* **18** 747 (2018)
35. Oulton R F *Mater. Today* **15** 26 (2012)
36. Vinogradov A P et al. *Phys. Usp.* **55** 1046 (2012); *Usp. Fiz. Nauk* **182** 1122 (2012)
37. Protsenko I E *Phys. Usp.* **55** 1040 (2012); *Usp. Fiz. Nauk* **182** 1116 (2012)
38. Ma R-M et al. *Laser Photon. Rev.* **7** 1 (2013)
39. Berini P, De Leon I *Nature Photon.* **6** 16 (2012)
40. Tame M S et al. *Nature Phys.* **9** 329 (2013)
41. Fitzgerald J M et al. *Proc. IEEE* **104** 2307 (2016)
42. Gwo S, Shih C-K *Rep. Prog. Phys.* **79** 086501 (2016)
43. Arnold N, Hrelescu C, Klar T A *Ann. Physik* **528** 295 (2016)
44. Premaratne M, Stockman M I *Adv. Opt. Photon.* **9** 79 (2017)
45. West P R et al. *Laser Photon. Rev.* **4** 795 (2010)
46. Bouillard J-S G et al. *Nano Lett.* **12** 1561 (2012)
47. Jayanti S V et al. *Opt. Mater. Express* **5** 1147 (2015)
48. Graedel T E *J. Electrochem. Soc.* **139** 1963 (1992)
49. Švorčík V et al. *J. Appl. Polymer Sci.* **99** 1698 (2006)
50. Etchegoin P G, Le Ru E C, Meyer M *J. Chem. Phys.* **125** 164705 (2006)
51. Beaglehole D et al. *Phys. Rev. B* **19** 6303 (1979)
52. Gao H W et al. *Proc. Natl. Acad. Sci. USA* **105** 20146 (2008)
53. Langhammer C et al. *Nano Lett.* **8** 1461 (2008)
54. Arnold M D, Blaber M G *Opt. Express* **17** 3835 (2009)
55. West P R et al. *Laser Photon. Rev.* **4** 795 (2010)
56. Boltasseva A, Atwater H A *Science* **331** 290 (2011)
57. Naik G V, Kim J, Boltasseva A *Opt. Mater. Express* **1** 1090 (2011)
58. Naik G V et al. *Opt. Mater. Express* **2** 478 (2012)
59. Khurgin J B, Boltasseva A *MRS Bull.* **37** 768 (2012)
60. Hryciw A, Jun Y C, Brongersma M L *Nature Mater.* **9** 3 (2010)
61. Soref R *Nature Photon.* **4** 495 (2010)
62. Cleary J W et al. *J. Opt. Soc. Am. B* **27** 730 (2010)
63. Naik G V, Shalaev V M, Boltasseva A *Adv. Mater.* **25** 3264 (2013)
64. Blaber M G, Arnold M D, Ford M J *J. Phys. Condens. Matter* **22** 143201 (2010)
65. Khurgin J B *Nature Nanotechnol.* **10** 2 (2015)
66. Khurgin J B, Sun G *Appl. Phys. Lett.* **96** 181102 (2010)
67. Baranov D G et al. *Opt. Express* **21** 10779 (2013)
68. Baranov D G et al. *Opt. Lett.* **38** 2002 (2013)
69. Gordon J A, Ziolkowski R W *Opt. Express* **15** 2622 (2007)
70. Larkin I A, Stockman M I *Nano Lett.* **5** 339 (2005)
71. Bohren C F, Huffman D R *Absorption and Scattering of Light by Small Particles* (New York: Wiley, 1983)
72. Liz-Marzán L M *Langmuir* **22** 32 (2006)
73. Tan S J et al. *Nature Nanotechnol.* **6** 268 (2011)
74. Ringe E et al. *Phys. Chem. Chem. Phys.* **15** 4110 (2013)
75. Mie G *Ann. Physik* **25** 377 (1908)
76. Maier S A *Plasmonics: Fundamentals and Applications* (New York: Springer, 2007)
77. Ruppin R *Surf. Sci.* **127** 108 (1983)
78. da Silva A G M et al. *Langmuir* **31** 10272 (2015)
79. Kumarasinghe C, Premaratne M, Agrawal G P *Opt. Express* **22** 11966 (2014)
80. Attanayake T, Premaratne M, Agrawal G *Plasmonics* **10** 1453 (2015)
81. Gersten J, Nitzan A *J. Chem. Phys.* **73** 3023 (1980)
82. Vernon K C et al. *Nano Lett.* **10** 2080 (2010)
83. Sikdar D et al. *Plasmonics* **9** 659 (2014)
84. Zhu W et al. *Plasmonics* **10** 881 (2015)
85. Sherry L J et al. *Nano Lett.* **5** 2034 (2005)
86. Sikdar D, Cheng W, Premaratne M *J. Appl. Phys.* **117** 083101 (2015)
87. da Silva A G M et al. *Langmuir* **31** 10272 (2015)
88. Barrow S J et al. *Nature Commun.* **3** 1275 (2012)
89. Das P, Chini T K, Pond J *J. Phys. Chem. C* **116** 15610 (2012)
90. Pérez-Juste J et al. *Coord. Chem. Rev.* **249** 1870 (2005)
91. Xiong W et al. *Chem. Commun.* **49** 9630 (2013)
92. Barrow S J et al. *Nature Commun.* **3** 1275 (2012)
93. Kang Z et al. *Opt. Express* **22** 19567 (2014)
94. Chang S-W, Ni C-Y A, Chuang S L *Opt. Express* **16** 10580 (2008)
95. Carbó-Argibay E et al. *Angew. Chem. Int. Ed.* **46** 8983 (2007)
96. Hao F et al. *Nano Lett.* **7** 729 (2007)
97. Pendry J B et al. *IEEE Trans. Microwave Theory Tech.* **47** 2075 (1999)
98. Linden S et al. *Science* **306** 1351 (2004)
99. Melentiev P N et al. *Nano Lett.* **16** 1138 (2016)
100. Flytzanis C et al., in *Progress in Optics* Vol. 29 (Ed. E Wolf) (Amsterdam: North-Holland, 1991) p. 321
101. Hu M et al. *J. Mater. Chem.* **18** 1949 (2008)
102. Blaber M G et al. *J. Phys. Chem. C* **116** 393 (2012)
103. Pile D F P et al. *App. Phys. Lett.* **87** 061106 (2005)
104. Bozhevolnyi S I et al. *Phys. Rev. Lett.* **95** 046802 (2005)
105. Steinberger B et al. *Appl. Phys. Lett.* **88** 094104 (2006)
106. Reinhardt C et al. *Opt. Lett.* **31** 1307 (2006)
107. Holmgaard T, Bozhevolnyi S I *Phys. Rev. B* **75** 245405 (2007)
108. Dionne J A, Lezec H J, Atwater H A *Nano Lett.* **6** 1928 (2006)
109. Verhagen E et al. *Phys. Rev. Lett.* **102** 203904 (2009)
110. Marell M J H et al. *Opt. Express* **19** 15109 (2011)
111. Lakhani A M et al. *Opt. Express* **19** 18237 (2011)
112. Rukhlenko I D et al. *Phys. Rev. B* **84** 113409 (2011)
113. Rukhlenko I D, Premaratne M, Agrawal G P *Adv. Opto-Electron.* **2012** 907183 (2012)
114. Handapangoda D et al. *Opt. Express* **19** 16058 (2011)
115. Handapangoda D, Rukhlenko I D, Premaratne M *J. Opt. Soc. Am. B* **29** 553 (2012)
116. Berini P *Phys. Rev. B* **61** 10484 (2001)
117. Zia R, Selker M D, Brongersma M L *Phys. Rev. B* **71** 165431 (2005)
118. Oulton R F et al. *Nature Photon.* **2** 496 (2008)
119. Oulton R F et al. *New J. Phys.* **10** 105018 (2008)
120. Takahara J et al. *Opt. Lett.* **22** 475 (1997)
121. Jung J, Søndergaard T, Bozhevolnyi S I *Phys. Rev. B* **76** 035434 (2007)
122. Goykhman I, Desiatov B, Levy U *Appl. Phys. Lett.* **97** 141106 (2010)
123. Sorger V J et al. *Nature Commun.* **2** 331 (2011)
124. Oulton R et al. *Nature Photon.* **2** 496 (2008)
125. Maier S A et al. *Adv. Mater.* **13** 1501 (2001)
126. Barrow S J et al. *Nano Lett.* **11** 4180 (2011)
127. Chen T et al. *J. Phys. Chem. Lett.* **4** 2147 (2013)
128. Esteban R et al. *Langmuir* **28** 8881 (2012)
129. Tserkezis C et al. *Part. Part. Syst. Charact.* **31** 152 (2014)
130. Baranov D G, Vinogradov A P, Lisyansky A A *J. Opt. Soc. Am. B* **32** 281 (2015)
131. Weber W H, Ford G W *Phys. Rev. B* **70** 125429 (2004)
132. Linden S, Kuhl J, Giessen H *Phys. Rev. Lett.* **86** 4688 (2001)
133. Maier SA, Kik P G, Atwater H A *Appl. Phys. Lett.* **81** 1714 (2002)
134. Brongersma M L, Hartman J W, Atwater H A *Phys. Rev. B* **62** R16356 (2000)
135. Maier S A et al. *Nature Mater.* **2** 229 (2003)
136. Lu J Q, Maradudin A A *Phys. Rev. B* **42** 11159 (1990)
137. Novikov I V, Maradudin A A *Phys. Rev. B* **66** 035403 (2002)

138. Moreno E et al. *Opt. Lett.* **23** 3447 (2006)
139. Bozhevolnyi S I et al. *Phys. Rev. Lett.* **95** 046802 (2005)
140. Oulton R F *Mater. Today* **15** 592 (2012)
141. Wang B, Wang G P *Appl. Phys. Lett.* **85** 3599 (2004)
142. Tanaka K, Tanaka M *Appl. Phys. Lett.* **82** 1158 (2003)
143. Veronis G, Fan S *J. Lightwave Technol.* **25** 2511 (2007)
144. Pile D F P, Gramotnev D K *Appl. Phys. Lett.* **86** 161101 (2005)
145. Sorger V J et al. *Nano Lett.* **9** 3489 (2009)
146. Oulton R F et al. *Nature* **461** 629 (2009)
147. Sorger V J, Zhang X *Science* **333** 709 (2011)
148. Bryant G W, García de Abajo F J, Aizpurua J *Nano Lett.* **8** 631 (2008)
149. Aizpurua J et al. *Phys. Rev. B* **71** 235420 (2005)
150. Zhang X-Y et al. *Opt. Express* **18** 18945 (2010)
151. Chu H-S et al. *Appl. Phys. Lett.* **96** 221103 (2010)
152. Lee K-S, El-Sayed M A *J. Phys. Chem. B* **110** 19220 (2006)
153. Sburlan S E, Blanco L A, Neito-Vesperinas M *Phys. Rev. B* **73** 035403 (2006)
154. Novotny L *Phys. Rev. Lett.* **98** 266802 (2007)
155. Nezhad M P et al. *Nature Photon.* **4** 395 (2010)
156. Schmucker A L et al. *ACS Nano* **4** 5453 (2010)
157. Bozhevolnyi S I, in *Plasmonic Nanoguides and Circuits* (Ed. S I Bozhevolnyi) (Singapore: World Scientific, 2009)
158. Zia R et al. *J. Opt. Soc. Am. A* **21** 2442 (2004)
159. Economou E N *Phys. Rev.* **182** 539 (1969)
160. Sarid D *Phys. Rev. Lett.* **47** 1927 (1981)
161. Burke J J, Stegeman G I, Tamir T *Phys. Rev. B* **33** 5186 (1986)
162. Berini P *Opt. Express* **14** 13030 (2006)
163. Dionne J A et al. *Phys. Rev. B* **72** 075405 (2005)
164. Boltasseva A et al. *J. Lightwave Technol.* **23** 413 (2005)
165. Plotz G A, Simon H J, Tucciarone J M *J. Opt. Soc. Am.* **69** 419 (1979)
166. Sirtori C et al. *Opt. Lett.* **23** 1366 (1998)
167. Tredicucci A et al. *App. Phys. Lett.* **76** 2164 (2000)
168. Nezhad M P, Tetz K, Fainman Y *Opt. Express* **12** 4072 (2004)
169. Seidel J, Grafstrom S, Eng L *Phys. Rev. Lett.* **94** 177401 (2005)
170. Noginov M A et al. *Opt. Express* **16** 1385 (2008)
171. Kumar P, Tripathi V K, Liu C S *J. Appl. Phys.* **104** 033306 (2008)
172. Noginov M A et al. *Phys. Rev. Lett.* **101** 226806 (2008)
173. Banerjee A, Li R, Grebel H *Appl. Phys. Lett.* **95** 251106 (2009)
174. Bolger P M et al. *Opt. Lett.* **35** 1197 (2010)
175. Ma R M et al. *Nature Mater.* **10** 110 (2011)
176. Kwon S-H et al. *Nano Lett.* **10** 3679 (2010)
177. Hill M T et al. *Opt. Express* **17** 11107 (2009)
178. Yariv A *Quantum Electronics* (New York: Wiley, 1989)
179. Verdeyen J T *Laser Electronics* (Englewood Cliffs, NJ: Prentice Hall, 1994)
180. Ambati M et al. *Nano Lett.* **8** 3998 (2008)
181. Noginov M A et al. *Phys. Rev. Lett.* **101** 226806 (2008)
182. De Leon I, Berini P *Nature Photon.* **4** 382 (2010)
183. Nair L G *Prog. Quantum Electron.* **7** 153 (1982)
184. Schafer F P *Dye Lasers* (Berlin: Springer-Verlag, 1990)
185. De Leon I, Berini P *Opt. Express* **17** 20191 (2009)
186. Osborne S W et al. *J. Phys. Condens. Matter* **16** S3749 (2004)
187. Wundke K et al. *Appl. Phys. Lett.* **76** 10 (2000)
188. Biasiol G, Heun S *Phys. Rep.* **500** 117 (2011)
189. Kirstaedter N et al. *Appl. Phys. Lett.* **69** 1226 (1996)
190. Müller J et al. *Appl. Phys. Lett.* **96** 131105 (2010)
191. Gather M C et al. *Nature Photon.* **4** 457 (2010)
192. Svendsen W, Ellegaard O, Schou J *Appl. Phys. A* **63** 247 (1996)
193. Melentiev P N et al. *Opt. Lett.* **38** 2274 (2013)
194. Melentiev P N et al. *Opt. Express* **21** 13896 (2013)
195. Melentiev P N et al. *Laser Phys. Lett.* **10** 075901 (2013)
196. Srinivasan K et al. *Opt. Express* **14** 1094 (2006)
197. Zhang J P et al. *Phys. Rev. Lett.* **75** 2678 (1995)
198. Huang M H et al. *Science* **292** 1897 (2001)
199. Park H et al. *Nature Phys.* **2** 484 (2006); Moody G et al. *Optica* **5** 395 (2018)
200. Genov D A et al. *Phys. Rev. B* **83** 245312 (2011)
201. Purcell E M, Torrey H C, Pound R V *Phys. Rev.* **69** 681 (1946)
202. Andrianov E S et al. *JETP Lett.* **97** 452 (2013); *Pis'ma Zh. Eksp. Teor. Fiz.* **97** 522 (2013)
203. Andrianov E S et al. *JETP* **117** 205 (2013); *Zh. Eksp. Teor. Fiz.* **144** 243 (2013)
204. Bennett A J et al. *Appl. Phys. Lett.* **90** 191911 (2007)
205. Song B-S et al. *Nature Mater.* **4** 207 (2005)
206. Altug H, Englund D, Vučković J *Nature Phys.* **2** 484 (2006)
207. Carmon T, Vahala K J *Nature Phys.* **3** 430 (2007)
208. Kinkhabwala A et al. *Nature Photon.* **3** 654 (2009)
209. Cho C-H et al. *Nature Mater.* **10** 669 (2011)
210. Sorger V J et al. *Nano Lett.* **11** 4907 (2011)
211. Yokoyama H et al. *Opt. Quantum Electron.* **24** S245 (1992)
212. Cassidy D T *J. Opt. Soc. Am. B* **8** 747 (1991)
213. Bjork G, Yamamoto Y *IEEE J. Quantum Electron.* **27** 2386 (1991)
214. Ambati M et al. *IEEE J. Sel. Top. Quantum Electron.* **14** 1395 (2008)
215. Khurgin J B, Sun G *Opt. Express* **20** 15309 (2012)
216. Schawlow A L, Townes C H *Phys. Rev.* **112** 1940 (1958)
217. Henry C H *IEEE J. Quantum Electron.* **18** 259 (1982)
218. Ginzburg P, Zayats A V *Opt. Express* **21** 2147 (2013)
219. Khajavikhan M et al. *Nature* **482** 204 (2012)
220. Hill M T et al. *Nature Photon.* **1** 589 (2007)
221. Wheeler H A *Proc. IRE* **35** 1479 (1947)
222. Stockman M I *J. Opt.* **12** 024004 (2010)
223. Duarte F J, Hillman L W (Eds) *Dye Laser Principles, with Applications* (Boston: Academic Press, 1990)
224. Vedantam S et al. *Nano Lett.* **9** 3447 (2009)
225. Vial S et al. *Langmuir* **23** 4606 (2007)
226. Garcia-Vidal F J, Moreno E *Nature* **461** 604 (2009)
227. Khurgin J B, Sun G *Nature Photon.* **8** 468 (2014)
228. Arnold N et al. *Opt. Mater. Express* **5** 2546 (2015)
229. Richter M et al. *Phys. Rev. B* **91** 035306 (2015)
230. Dionne J A, Lezec H J, Atwater H A *Nano Lett.* **6** 1928 (2006)
231. Pile D F P et al. *Opt. Express* **15** 13669 (2007)
232. Ma R M, Dai L, Qin G G *Appl. Phys. Lett.* **90** 093109 (2007)
233. Lu Y-J et al. *Nano Lett.***14** 4381 (2014)
234. Kovacs G J *Thin Solid Films* **60** 33 (1979)
235. Fukui M, So V C Y, Normandin R *Phys. Status Solidi B* **91** K61 (1979)
236. Ding K et al. *Phys. Rev. B* **85** 041301(R) (2012)
237. Ding K et al. *Opt. Express* **21** 4728 (2013)
238. Ding K et al. *Appl. Phys. Lett.* **98** 231108 (2011)
239. Ding K et al. *Appl. Phys. Lett.* **102** 041110 (2013)
240. Stehr J et al. *Adv. Mater.* **15** 1726 (2003)
241. van Beijnum F et al. *Phys. Rev. Lett.* **110** 206802 (2013); Stockman M I et al. *J. Opt.* **20** 043001 (2018)
242. Suh J Y et al. *Nano Lett.* **12** 5769 (2012)
243. Zhou W et al. *Nature Nanotechnol.* **8** 506 (2013)
244. de Waele R, Koenderink A F, Polman A *Nano Lett.* **7** 2004 (2007)
245. Quinten M A et al. *Opt. Lett.* **23** 1331 (1998)
246. Engheta N, Salandrino A, Alù A *Phys. Rev. Lett.* **95** 095504 (2005)
247. Citrin D S *Nano Lett.* **4** 1561 (2004)
248. Koenderink A F, Polman A *Phys. Rev. B* **74** 033402 (2006)
249. Zheludev N I et al. *Nature Photon.* **2** 351 (2008)
250. Schokker A H, Koenderink A F *Phys. Rev. B* **90** 155452 (2014)
251. Gao H et al. *Opt. Express* **17** 2334 (2009)
252. Yang A et al. *Nature Commun.* **6** 6939 (2015)
253. Yang A et al. *ACS Nano* **9** 11582 (2015)
254. Melentiev P N et al. *Laser Phys. Lett.* **11** 105301 (2014)
255. Zyablovsky A A et al. *AIP Conf. Proc.* **1475** 185 (2012)
256. Dorofeenko A V et al. *Opt. Express* **21** 14539 (2013)
257. Wu C et al. *Optica* **3** 734 (2014)
258. Melentiev P et al. *Appl. Phys. Lett.* **111** 213104 (2017)
259. Ahmed Z et al. *J. Phys. Commun.* **2** 045016 (2018)
260. Meng X et al. *Laser Photon. Rev.* **8** 896 (2014)
261. Srinivasan K et al. *Opt. Express* **14** 1094 (2006)
262. Ning C Z *Phys. Status Solidi B* **247** 774 (2010)
263. Ellis B et al. *Nature Photon.* **5** 297 (2011)
264. Siegman A E *Lasers* (Mill Valley, Calif.: Univ. Science Books, 1986)
265. Milonni P W, Eberly J H *Laser Physics* (New York: John Wiley and Sons, 2010)
266. Miyazaki H T, Kurokawa Y *Phys. Rev. Lett.* **96** 097401 (2006)
267. Kien F L et al. *Opt. Commun.* **242** 445 (2004)
268. Kien F L et al. *Phys. Rev. A* **72** 032509 (2005)
269. Coulon P M et al., *Opt. Express* **25** 28246 (2017)
270. Lu C-Y et al. *IEEE Photon. Technol. Lett.* **23** 1031 (2011)

271. Yu K, Lakhani A, Wu M C *Opt. Express* **18** 8790 (2010)
272. Tong L et al. *Nature* **426** 816 (2003)
273. Barnes W L, Dereux A, Ebbesen T W *Nature* **424** 824 (2003)
274. Stockman M *Opt. Express* **19** 22029 (2011)
275. Miller S E *Bell Syst. Tech. J.* **48** 2059 (1969)
276. Ishii S, Nakagawa A, Baba T IEEE *J. Sel. Top. Quantum Electron.* **12** 71 (2006)
277. Hill M T et al. *Nature* **432** 206 (2004)
278. Miller D A B *Proc. IEEE* **97** 1166 (2009)
279. Beausoleil R G et al. *Proc. IEEE* **96** 230 (2008)
280. Pan L, Bogy D B *Nature Photon.* **3** 189 (2009)
281. Leuthold J et al. *Opt. Photon. News* **24** 28 (2013)
282. Balykin V I et al. *Phys. Rev. A* **70** 011401(R) (2004)
283. Lončar M, Scherer A, Qiu Y M *Appl. Phys. Lett.* **82** 4648 (2003)
284. Kano H, Kawata S *Opt. Lett.* **21** 1848 (1996)
285. Nie S, Emory S R *Science* **275** 1102 (1997)
286. Kneipp K et al. *Phys. Rev. Lett.* **78** 1667 (1997)
287. Danckwerts M, Novotny L *Phys. Rev. Lett.* **98** 026104 (2007)
288. Anker J N et al. *Nature Mater.* **7** 442 (2008)
289. Hill R T et al. *Nano Lett.* **10** 4150 (2010)
290. Lozovik Yu E, Nechepurenko I A, Dorofeenko A V *Photon. Nanostruct. Fundam. Appl.* **21** 60 (2016)
291. Brolo A G *Nature Photon.* **6** 709 (2012)
292. Li Z-Y, Xia Y *Nano Lett.* **10** 243 (2010)
293. Ma R-M et al. *Nature Nanotechnol.* **9** 600 (2014)
294. Rochat S, Swager T M *ACS Appl. Mater. Interfaces* **5** 4488 (2013)
295. Sauer M, Hofkens J, Enderlein J *Handbook of Fluorescence Spectroscopy: From Ensemble to Single Molecule* (New York: John Wiley and Sons, 2011)
296. Hell S W *Nature Meth.* **6** 24 (2009)
297. Huang X et al. *Nanomedicine* **2** 681 (2007)
298. de la Zerda A et al. *Contrast Media Mol. Imaging* **6** 346 (2011)
299. Stockman M I *Science* **348** 287 (2015)
300. Galanzha E I et al. *Nature Commun.* **8** 15528 (2017)
301. Smit M, van der Tol J, Hill M *Laser Photon. Rev.* **6** 1 (2012)
302. Ni C-Y A, Chuang S L *Opt. Express* **20** 16450 (2012)
303. Takeda K et al. *Nature Photon.* **7** 569 (2013)
304. Ma R-M et al. *Nano Lett.* **12** 5396 (2012)
305. Challener W A et al. *Nature Photon.* **3** 220 (2009)
306. Stipe B et al. *Nature Photon.* **4** 484 (2010)
307. Nakayama Y et al. *Nature* **447** 1098 (2007)
308. Srituravanich W et al. *Nature Nanotechnol.* 3 733 (2008)
309. Kim Y et al. *Opt. Express* **17** 19476 (2009)
310. Xie Z et al. *Plasmonics* **6** 565 (2011)